


ROCK2 inhibition triggers the collective invasion of colorectal adenocarcinomas

Fotine Libanje¹, Joel Raingeaud¹, Rui Luan¹, Zoé Ap Thomas¹, Olivier Zajac^{1,†}, Joel Veiga^{2,‡}, Laetitia Marisa³, Julien Adam⁴, Valerie Boige⁵, David Malka⁵, Diane Goéré⁵, Alan Hall², Jean-Yves Soazec⁴, Friedrich Prall⁶, Maximiliano Gelli⁵, Peggy Dartigues⁴ & Fanny Jaulin^{1,*} 

Abstract

The metastatic progression of cancer is a multi-step process initiated by the local invasion of the peritumoral stroma. To identify the mechanisms underlying colorectal carcinoma (CRC) invasion, we collected live human primary cancer specimens at the time of surgery and monitored them *ex vivo*. This revealed that conventional adenocarcinomas undergo collective invasion while retaining their epithelial glandular architecture with an inward apical pole delineating a luminal cavity. To identify the underlying mechanisms, we used microscopy-based assays on 3D organotypic cultures of Caco-2 cysts as a model system. We performed two siRNA screens targeting Rho-GTPases effectors and guanine nucleotide exchange factors. These screens revealed that ROCK2 inhibition triggers the initial leader/follower polarization of the CRC cell cohorts and induces collective invasion. We further identified FARP2 as the Rac1 GEF necessary for CRC collective invasion. However, FARP2 activation is not sufficient to trigger leader cell formation and the concomitant inhibition of Myosin-II is required to induce invasion downstream of ROCK2 inhibition. Our results contrast with ROCK pro-invasive function in other cancers, stressing that the molecular mechanism of metastatic spread likely depends on tumour types and invasion mode.

Keywords collective migration; colorectal carcinoma; GTPases; invasion; leader cells

Subject Categories Cancer; Cell Adhesion, Polarity & Cytoskeleton; Signal Transduction

DOI 10.15252/embj.201899299 | Received 22 February 2018 | Revised 19 April 2019 | Accepted 10 May 2019 | Published online 18 June 2019

The EMBO Journal (2019) 38: e99299

Introduction

With 90% of cancer patients succumbing from their metastases, there is a pressing need to understand the mechanisms of cancer cell dissemination (Ferlay *et al* 2015). Worsening patient prognosis and impacting medical treatments, the transition from *in situ* to invasive tumours is a crucial step in the metastatic progression that is triggered by the acquisition of migratory properties.

Cancer cell invasion has long been considered as a single-cell process (Valastyan & Weinberg, 2011) as observed in leukaemia, in loosely organized tissues like sarcomas, or in highly cohesive carcinomas that have undergone an epithelial-to-mesenchymal transition (EMT) (Friedl & Alexander, 2011). Activated by specific transcription factors (EMT-TFs), Twist, Zeb, Snail and Slug, the EMT programme promotes mesenchymal cell invasion, but also increases stemness and survival, all contributing to cancer development and metastatic progression (Thiery *et al*, 2009; Puisieux *et al*, 2014). Recently, mice models of breast and pancreas cancers have shown that EMT activation contributes to chemoresistance but is dispensable for metastases formation (Fischer *et al*, 2015; Zheng *et al*, 2015a). The participation of EMT-TFs and individualized dedifferentiated single cells to cancer metastatic dissemination is therefore highly debated (Nieto *et al*, 2016; Aiello *et al*, 2017; Krebs *et al*, 2017; Ye *et al*, 2017).

Cancer cell clusters can also invade as cohesive groups, a process called collective invasion. First observed from primary tumour explants over 20 years ago (Friedl *et al*, 1995), the collective invasion of cancer cells has been confirmed over the past decade by intravital microscopy in a variety of experimental model systems (Friedl, 2004; Alexander *et al*, 2008; Giampieri *et al*, 2009) and the systematic prospective analysis of primary tumour explants (Zajac *et al*, 2018). Yet, the cellular and molecular mechanisms underlying this process have been poorly investigated and most of our knowledge is based on the collective migration driving the embryonic

¹ INSERM U-981, Gustave Roussy, Villejuif, France

² Cell Biology Program, Memorial Sloan-Kettering Cancer Center, New York, NY, USA

³ Programme "Cartes d'Identité des Tumeurs", Ligue Nationale Contre le Cancer, Paris, France

⁴ Pathology Department, Gustave Roussy, Villejuif, France

⁵ Digestive Cancer Unit, Gustave Roussy, Villejuif, France

⁶ Institute of Pathology, University Medicine of Rostock, Rostock, Germany

*Corresponding author. Tel: +33 1 4211 5068; E-mail: fanny.jaulin@gustaveroussy.fr

†Present address: Department of Translational Research, Curie Institute, Paris, France

‡Present address: Imagine Institute, Paris, France

development of model organisms. The front-rear polarization of the moving cohort translates into distinct cells, the leaders and the followers, cooperating to tract the collective (Haas & Gilmour, 2006; Wang *et al*, 2010). The leaders, protrusive cells at the front, respond to extracellular guiding cues and adhere to the matrix to generate traction forces. They are either defined by their closest position relative to the chemokine gradient, such as in *drosophila* border cells or mammalian vascular sprouting (Duchek *et al*, 2001) or by the expression of a transcriptional programme pre-existing to the migration process such as in zebrafish lateral line (Haas & Gilmour, 2006; Aman & Piotrowski, 2008) and in breast and lung carcinoma models (Cheung *et al*, 2013; Westcott *et al*, 2015; Konen *et al*, 2017).

As central regulators of the cytoskeleton, the small GTPases of the Rho family and their regulation by guanine nucleotide exchange factors (GEFs) and GTPase activating proteins (GAPs) play important functions in all modes of cell migration (Ridley, 2015). The balance between endogenous RhoA and Rac1 activities regulates the switch between the mesenchymal and the amoeboid mode of single-cell invasion (Sahai & Marshall, 2003; Wolf *et al*, 2003; Sanz-Moreno *et al*, 2008). The GEFs and GAPs balancing the activation of these small GTPases vary with cell types, and many of them have been shown to participate in invasion (Tsuji *et al*, 2002; Ohta *et al*, 2006; Even-Ram *et al*, 2007; Sanz-Moreno *et al*, 2008). Rho-GTPases activities were also shown to be crucial in leader cell and at the cell–cell junctions of collectively moving cells. Tissue-specific GEFs control the polarized activation of either Rac1 or Cdc42 in leader cells *in vitro* and *in vivo* (Osmani *et al*, 2006, 2010; Bianco *et al*, 2007; Migeotte *et al*, 2010; Wang *et al*, 2010; Ellenbroek *et al*, 2012; Cai *et al*, 2014; Omelchenko *et al*, 2014; Westcott *et al*, 2015; Yamaguchi *et al*, 2015). In contrast, the collective invasion of tumour spheres with inverted polarity (TSIPs) in hypermethylated colorectal carcinomas is independent of Rac1 and protruding leader cells (Zajac *et al*, 2018). In follower cells, the level of RhoA-GTP is tightly controlled at cell–cell contacts in order to relax the junctions while maintaining the communication and the cohesion of the group during the migration (Omelchenko & Hall, 2012; Omelchenko *et al*, 2014; Reffay *et al*, 2014; Zaritsky *et al*, 2017).

With 1 million new cases worldwide per year, colorectal carcinoma (CRC) is an important public health issue. CRCs develop through a series of genetic, genomic and epigenetic events along two distinct pathways: the CpG islands methylator phenotype (CIMP) generates microsatellite instability (MSI-high) or not (MSS or MSI-low) and gives rise to different histological subtypes, including mucinous and micropapillary CRCs (Yamane *et al*, 2014). The chromosomal instability pathway (CIN) is initiated by APC loss of function and leads to numerous chromosomes losses and amplifications (Pino & Chung, 2010). This neoplastic transformation is associated with the most common histological form of CRCs, named

“Lieberkuhnian” (LBK) or “not otherwise specified” (NOS). Large-scale transcriptomic analyses have defined the consensus molecular subtypes (CMSs) of CRCs, and one of the four groups is associated with poor patient prognosis and mesenchymal signature (Guinney *et al*, 2015). However, immunostaining of patient specimens and data collected from patient-derived xenografts support that the upregulation of mesenchymal genes actually occurs in the stroma rather than in the tumour through EMT activation (Calon *et al*, 2015; Matano *et al*, 2015; McCorry *et al*, 2018). Histological studies proved that tumour budding (clusters of 5 tumour cells or less) at the invasive front is an independent prognostic factor for CRC patients survival (Prall *et al*, 2005). Yet, the 3D reconstruction of tissue sections revealed that virtually all tumour buds are connected to the main tumour mass and it is impossible to assess whether they represent a reservoir of migratory cells moving as small unit or releasing individuals (Bronsert *et al*, 2014; Enderle-Ammour *et al*, 2017). Xenografted mice models of CRC have shown that silencing Zeb1 reduces metastases formation (Spaderna *et al*, 2008; Wellner *et al*, 2009). In contrast, transgenic mice expressing Fascin, a WNT/ β -catenin target gene, show that collective invasion also mediates CRC spread (Vignjevic *et al*, 2007). Therefore, the restriction of histological approaches based on fixed 2D cancer specimens and molecular analyses that cannot distinguish between tumour and stromal compartment have been unable to resolve the invasive behaviour of human CRCs. In this study, we monitored live cancer specimens *ex vivo* and identified that NOS colorectal adenocarcinomas predominantly undergo collective invasion in the form of differentiated epithelial glands. We then investigated how Rho-GTPases signalling triggers the formation of leader cells to promote the migration of these differentiated neoplastic cell cohorts.

Results

Conventional colorectal adenocarcinomas undergo collective invasion

To determine the mode of invasion involved in the early step of conventional (NOS) colorectal adenocarcinoma dissemination, we first analysed formalin-fixed paraffin-embedded (FFPE) surgical specimens from 16 human primary tumours that have invaded the submucosa (NOS, stage pT1, see Fig EV1A for patients, Fig EV1B for tumour characteristics and Fig 1Ai for a representative example). E-cadherin localized at cell–cell contact of both normal and transformed epithelial cell sheets (Fig 1Aii and iii and Fig EV1C). This staining highlighted the epithelial glandular organization of the neoplastic tissue, including the invasive front, with cohesive cancer cells surrounding a small luminal space (Fig 1Aii and iii). Between

Figure 1. Colorectal adenocarcinomas organize as cohesive and polarized epithelial glands.

- Representative specimen of colorectal (CRC) primary tumour stained with haematoxylin/eosin/saffron (HES), or antibodies against E-cadherin or vimentin. (i) The blue, orange and pink dotted lines highlight the normal mucosa, the submucosa and the muscularis propria, respectively. Red dotted line highlights the neoplastic tissue. Black arrowheads indicate the direction of invasion. Boxed regions ii and iii show high magnification of normal colonic glands (ii) and the CRC invasive front (iii). Scale bar: 2 mm and 500 μ m.
- Representative images of histological sections of normal colon and primary CRC stained for EpCam and Villin. Boxed regions i, ii and iii are high magnifications of the luminal cavity of normal colonic gland (i) and colorectal carcinoma glands (ii and iii). Arrow heads point to the apical pole enriched in villin. Scale bars: 50 μ m.
- Graph presenting the percentage of the tumour area displaying a glandular architecture from a cohort of 16 patients (see Fig EV1).

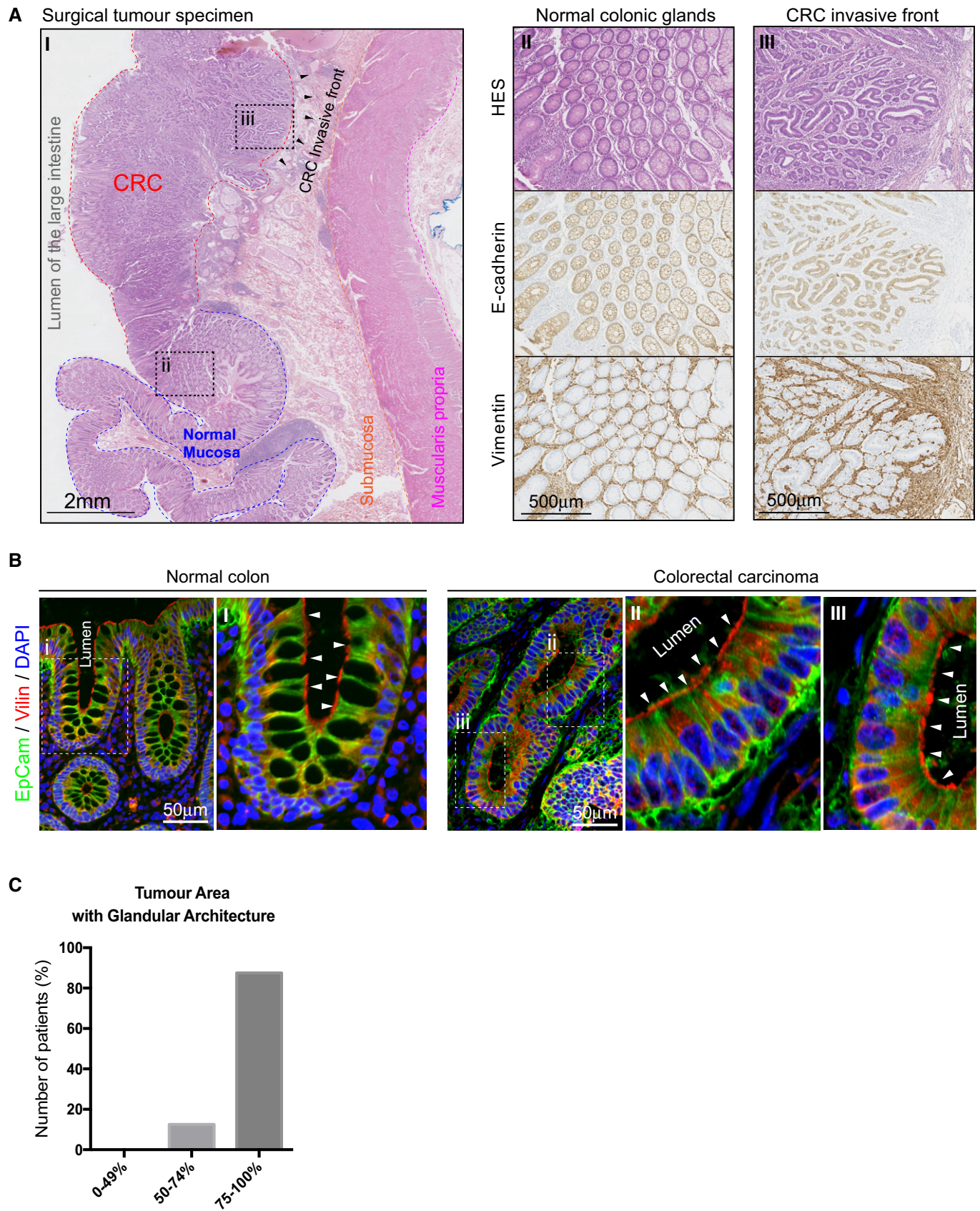


Figure 1.

these neoplastic glands, stromal cells display a robust vimentin staining (Vim+), Fig 1Aii and iii). Although we do not exclude that some Vim(+) cells could be CRC cells that have completely lost E-

cadherin expression and localize among the normal stromal cells, most of the tumour is organized as a cohesive tissue with E-cadherin-based junctions. This architecture suggested that CRCs

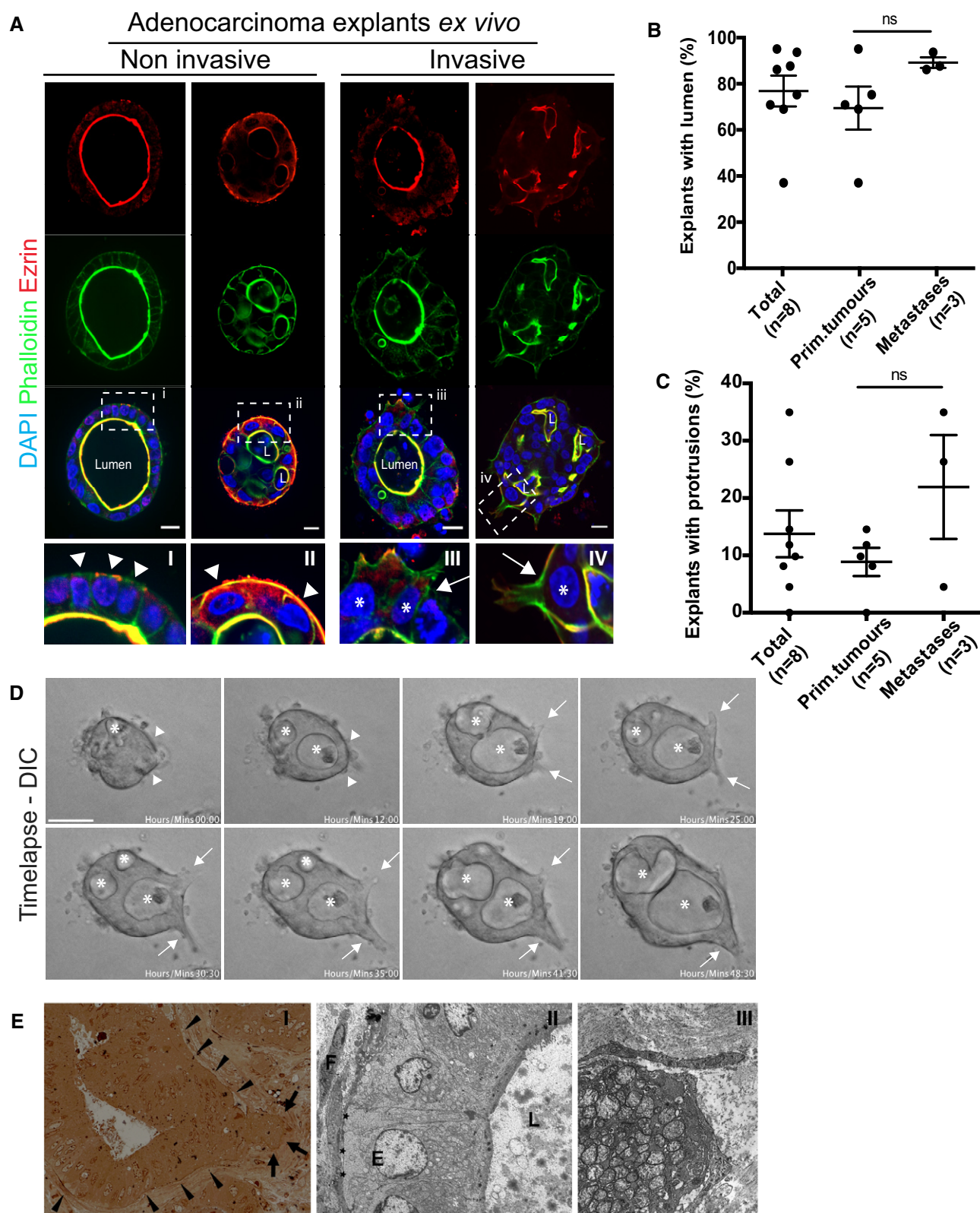


Figure 2.

Figure 2. Colorectal adenocarcinomas explants undergo collective invasion.

- A Representative confocal images of non-invasive or invasive human colorectal cancer explants collected from 8 patients with NOS adenocarcinoma (Fig EV2A and B). The explants were fixed 4 days after recovery and stained for the lumen (ezrin), F-actin (Phalloidin) and nuclei (DAPI). Boxed regions i, ii, iii and iv are displayed at high magnification. Arrowheads point to non-protruding cells, arrows point to protruding cells, and white stars show off-centred nuclei. Scale bars: 20 μ m.
- B, C Graphs representing the percentage of adenocarcinoma explants displaying lumens (B) or protrusions (C) from eight patients. Evaluation performed from DIC observation of live tissues, at least 50 explants were analysed per patients. The error bar represents the standard error of the mean (means \pm SEM). *P* values were calculated using unpaired *t*-test (ns: non-significant).
- D Time-lapse sequences of an adenocarcinoma explant undergoing collective invasion into collagen-I gel monitored by DIC microscopy over 2 days (corresponding to Movie EV1). Arrowheads point to non-protruding cells, arrows point to protruding cells, and white stars point to lumens. Scale bars: 50 μ m.
- E Images of an invading gland of a colorectal NOS adenocarcinoma, at the light microscopic level (i, semi-thin section, 100 \times objective), and as seen by electron microscopy (ii, 1,000 \times magnification; and iii, 4,000 \times magnification). Note that the bulk of the invading neoplastic gland is in a state of glandular organization (regions denoted by arrowheads in the left panel): epithelia (E, middle panel) are polarized to form a lumen (L) and are attached to a basal membrane (asterisk) by hemidesmosomes; the gland is surrounded by fibroblasts (F). However, this organization is focally disrupted at the tubular invasion pole (arrows in the left panel) where neoplastic epithelial cells have lost polarization and directly contact the surrounding stroma as the basal membrane is missing (right panel).

may maintain their differentiated features and apico-basolateral polarity during invasion. In support to this, immunostaining revealed the polarized localization of the apical marker villin at the plasma membrane facing the luminal cavity of normal and transformed epithelial glands (Fig 1B, arrowheads). The cell–cell adhesion molecule EpCam is excluded from the apical membrane and rather localizes at the basolateral compartment in contact with adjacent cancer cells and the basal lamina (Fig 1B). Histological assessment by pathologists revealed that in 87% of the patients (14/16), more than 75% of the tumour surface organized as glandular structure (Figs 1C and EV1B and C). This shows that tumour cells at the invasive front of pT1 colorectal adenocarcinomas maintain their cohesion and epithelial identity, preferentially organizing as glandular structures in the peritumoral stroma.

The presence of differentiated neoplastic cell cohorts at the invasive front could either result from single-cell invasion and sequential EMT and MET activation or from the collective migration of transformed tissues. To assess the dynamic invasive behaviour of colorectal adenocarcinoma, we monitored live tumour specimens by videomicroscopy. We retrieved primary tumour and metastases explants for 10 patients (Fig EV2A) the day of the cytoreductive surgery and immediately embedded them into tridimensional (3D) gel made of extracellular matrices (ECM). Four days after recovery, we performed time-lapse imaging during 48 h and stained for actin and ezrin at end point. CRC histotype assessment indicated that 2 out of 10 patients had mucinous CRC, correlating with the inverted apico-basolateral polarity of the explants we observed *ex vivo* and consistent with our previous study (Zajac *et al*, 2018) (Figs EV2A and EV2B, patients #E and #H, excluded from the present study focusing on NOS adenocarcinomas). For all patients with adenocarcinoma (8/8), all tumour explants remained cohesive and most displayed one or multiple lumens ($77.7 \pm 6.3\%$ and $81.6 \pm 4.9\%$ visualized by DIC or ezrin staining, respectively, Figs 2A and B, EV2C and D). We very rarely saw the detachment of single cells (not shown) and rather observed evident collective behaviour with cell groups protruding into the collagen-I gel (Fig 2C and D and Movie EV1). An average of $14 \pm 4\%$ of the explants harboured prominent actin-rich protrusions (Fig 2A arrows and 2C), contrasting with the smooth periphery of the non-invasive ones (Fig 2A (arrowheads), Fig EV2E and Movie EV2). The proportion of protruding explants varies between patients, ranging from 0 to 35%, but we did not detect a significant difference between primary tumours and metastases (Fig 2C). The polarized morphology of the invading

gland, with protruding cells harbouring the features of leaders, is not an *ex vivo* artefact from experimental procedures. Indeed, microscopic study of colorectal adenocarcinoma specimens obtained from the invasive margins by serial semi-thin sections, complemented by electron microscopy, showed that the highly organized state of differentiated neoplastic glands is disrupted focally in “tubular invasion poles” which appears to be the leading edge of invading glands (Fig 2Ei). In the fully formed parts of the neoplastic glands, the epithelia are polarized and abut a basal membrane resembling normal crypts (Fig 2Ei arrowheads and Fig 2Eii). However, at the invasion pole, the basal membrane is missing and “leader” epithelial cells form villiform cytoplasmic extensions in direct contact with the extracellular matrix (Fig 2Ei arrows and Fig 2Eiii). Taken together, the results we obtained from the analyses of fixed and live human primary cancer specimens revealed that NOS CRC maintain their apico-basolateral polarity and epithelial architecture as they collectively invade into the submucosa in the form of neoplastic glands. The focal formation of protruding leader cells seems to be the starting points for this process.

ROCK inhibition triggers collective invasion from Caco-2 cysts

To investigate the signalling pathways regulating adenocarcinoma collective invasion, we first sought an *in vitro* experimental model system that recapitulates the features we observed from tumour explants. We grew the CIN CRC cell line Caco-2 in 3D ECM gel. Immunostaining for the apical marker prominin-1 and F-actin revealed that Caco-2 cysts are formed by a polarized monolayer of cells surrounding a central lumen as seen in patients’ specimens. Over 90% of Caco-2 cysts harbour a smooth periphery due to the absence of protruding cells (Fig 3A, left panel, Movie EV3). As such, Caco-2 cysts grown in 3D matrices represent a pertinent organotypic model of non-invasive NOS adenocarcinoma, allowing gain-of-function studies to decipher the mechanisms triggering glandular collective invasion. To this end, we performed a siRNA-based screen targeting the RhoGTPase signalling pathway, central to all modes of cell motility. We transfected Caco-2 cells using a siRNA library targeting the 98 known human RhoGTPase effectors. Accounting for functional redundancy between homologs, we co-depleted the closest pair of proteins (Table EV1). We verified that the co-transfection of two siRNAs does not hinder the depletion of each protein (data not shown). The screen yielded three hits: Caco2 cysts transfected with siPARD6A+PDE6D developed a

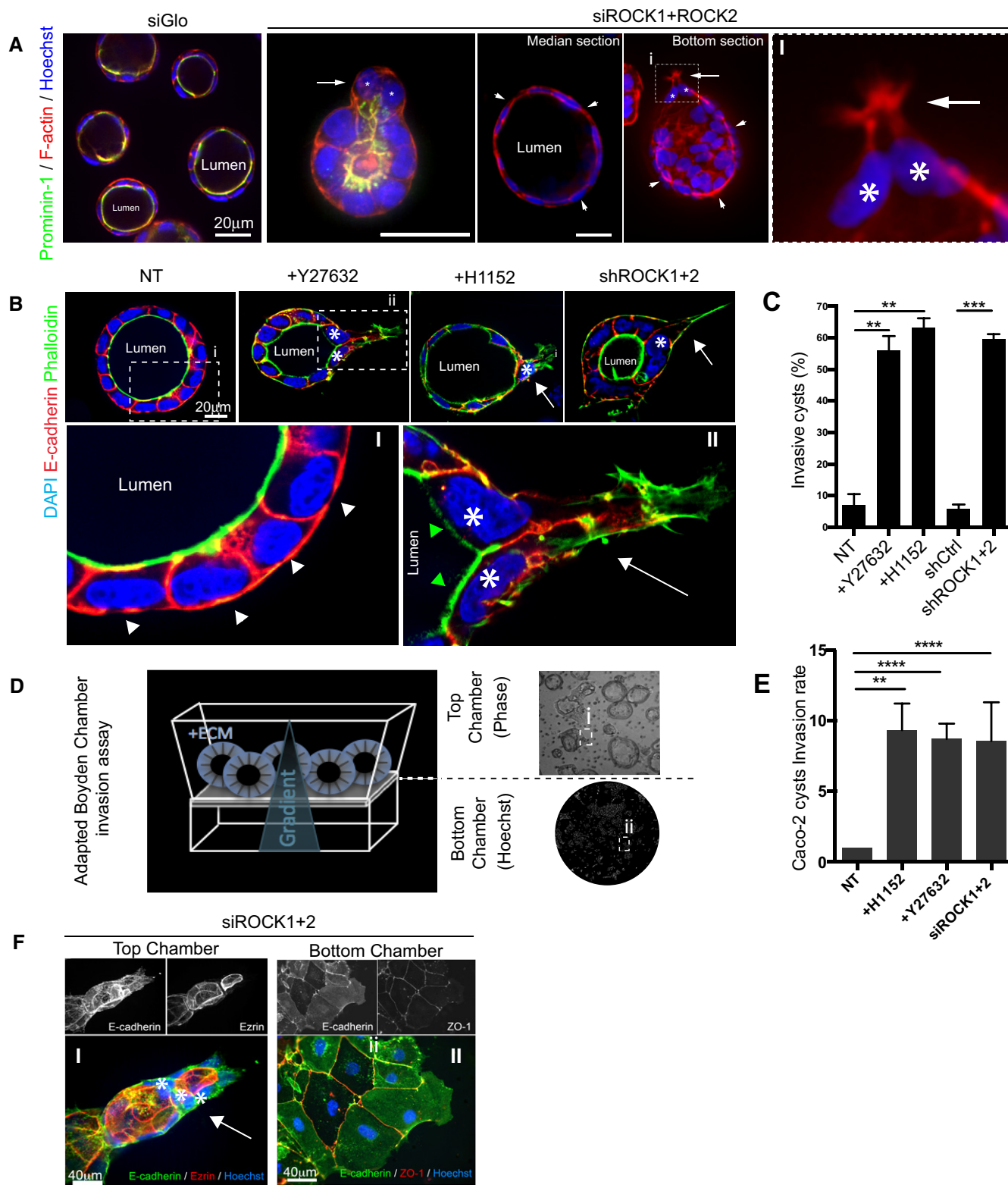


Figure 3.

multi-lumen phenotype (consistent with previous report; Durgan *et al*, 2011) and siPLXNA1+siPLD1 gave defective lumens (not shown). Caco-2 cysts co-depleted for ROCK1 and ROCK2 displayed

a supracellular polarization: a subset of protruding cells, usually two neighbours, get off-centred but remained attached to the cyst (Fig 3A, middle panels, arrows). Their nuclei lost the alignment

Figure 3. ROCK inhibition induces the collective invasion of Caco-2 cysts.

- A Representative images of Caco-2 cysts transfected with control siRNA (siGlo) or siRNAs targeting ROCK1 and ROCK2, fixed and stained for prominin-1, F-actin (Phalloidin) and nuclei (Hoechst). Confocal Z-sections of cysts are displayed. Arrowheads show non-protruding cells. Arrows point to protruding cells. White stars mark nuclei that are off-centred relative to the cyst's monolayer. Scale bars: 20 μ m.
- B Representative confocal images of Caco-2 cysts treated with ROCK inhibitors Y27632 and H1152, non-treated (NT) or transduced with ROCK1 and ROCK2 shRNAs (shROCK1+2). The cysts were fixed 2 days after invasion and stained for E-cadherin, F-actin (Phalloidin) and nuclei (DAPI). Boxed regions i and ii are displayed at high magnification. White arrowheads point to non-protruding cells, green arrowheads point to the apical pole, arrows point to protruding cells, and white stars show off-centred nuclei. Scale bar: 20 μ m.
- C Bar graph representing the percentage of protrusive Caco-2 cysts from three independent experiments. Caco-2 cysts non-treated (NT), incubated with ROCK inhibitors Y27632 and H1152 or infected with lentiviruses encoding shRNA control and targeting ROCK1 and ROCK2. The cysts were fixed 2 days after invasion; over 100 cysts were counted for each condition. Error bar represents the standard error of the mean (means \pm SEM). *P* values were calculated using unpaired *t*-test (***P* < 0.001, ****P* < 0.0001).
- D (Left panel) Schematic representation of the 3D Boyden chamber invasion assay. The Caco-2 was grown as cysts in 3D Matrigel on the top chamber of the Boyden for 3 days, and then, the serum gradient was induced. Two days after, the nuclei of the cells that have reached the bottom side of the membrane were stained with Hoechst and quantified by automated acquisition and segmentation. (Right panel) DIC image of the membrane facing the top chamber reveals the cysts and the immunofluorescence image of the membrane facing the bottom chamber stained with Hoechst reveals the cells that have invaded.
- E The number of cells that have invaded from the top to the bottom chamber of the Boyden chamber was quantified by automated segmentation in non-treated (NT), in ROCK inhibited conditions (Y27632, H1152) or in cells transfected with siRNA against ROCK1 and ROCK2 (siROCK1+2). The number of cells that have invaded was normalized to control conditions and reported as the average invasion rate from at least three independent experiments (means \pm SEM). *P* values were calculated using unpaired *t*-test (*****P* < 0.0001, ***P* < 0.01).
- F High magnification of boxed region from (D). The top (i) and the bottom (ii) side of the Boyden chamber membrane was stained for F-actin, E-cadherin, ZO-1, ezrin and Hoechst. Arrow points to the protrusive cells of an invasive cyst, and the white stars show the nuclei that engage in the protrusion. Scale bars: 40 μ m.

with the monolayer and engaged into protrusion (Fig 3A, middle panel, stars). In a validation round, Z-stacks acquisition of Caco-2 cysts transfected with siROCKs further demonstrated that the bulging cells formed actin-rich protrusions towards the ECM gel (Fig 3A (right panels, arrows) and Fig EV3A), while the rest of the cohort did not (Fig 3A, arrowheads). These protruding morphology and supracellular polarization of Caco-2 cysts transfected with siRNA targeting ROCK resemble the collective invasion pattern observed from the CRC explants (Fig 2A). To confirm this result and exclude an off-target effect of the siRNAs, we used alternative reagents. First, we transduced Caco-2 cysts using shRNAs against ROCK1 and ROCK2 (Fig EV3B). This induced a 10-fold increase in the number of cysts with protruding cells, raising from $6 \pm 1\%$ to $60 \pm 1\%$, demonstrating the phenotype was specific to ROCK depletion (Fig 3B and C). We then used pharmacological inhibitors Y27632 and H1152 to determine whether ROCK kinase activity was sufficient to control this phenotype. Treatment with Y27632 and H1152, respectively, increased the number of protruding cysts from $7 \pm 2\%$ to $56 \pm 3\%$ and $63 \pm 2\%$ (Fig 3B and C). Using live imaging, we confirmed that the “leader/follower” polarization of Caco-2 cysts treated with ROCK inhibitors Y27632 and H1152 resulted from the neoformation of protrusions, as observed from patient explants (Fig EV3C). E-cadherin staining confirmed that all cells of the cohort remained cohesive and that the luminal cavity was conserved (Fig 3B).

To determine whether the “leader/follower” polarization of protruding Caco-2 cysts efficiently translates into invasion, we adapted the Boyden chamber to 3D organotypic cultures. The membrane was coated with Matrigel, and Caco-2 cells were grown as cysts in 3D gels in the top chamber. To allow chemotacticism, a serum gradient was established from the bottom chamber (Fig 3D). In this new assay, we evaluated the ability of Caco-2 cells to invade from the top to the bottom chamber of the Transwell. The number of cells that have invaded was analysed by automated segmentation and quantification 3 days after induction of the serum gradient. As expected for a non-invasive CRC model, very few Caco-2 cells reached the bottom chamber in control condition. In contrast,

treatment with Y27632 and H1152 or transfection of siROCKs increased by 9.3 ± 1.9 -, 8.7 ± 1.1 - and 8.5 ± 2.7 -fold, respectively, the number of cells reaching the bottom chamber (Fig 3E). Immunostaining of the top and bottom side of the membrane using antibodies against E-cadherin, ZO-1 and ezrin demonstrated that Caco-2 cells remain cohesive in both compartments (Fig 3F). In support to this, we did not detect any change in the expression level of epithelial (E-cadherin and keratins) and mesenchymal (N-cadherin and vimentin) markers, showing that the acquisition of the invasive phenotype occurs independently of the activation of an EMT programme (Fig EV3D). Hence, inhibiting ROCK kinase activity is sufficient to trigger protruding activity and collective invasion from Caco-2 cysts.

Inhibiting ROCK activity augments collective invasion from colorectal adenocarcinoma explants

To confirm ROCK function, we first examined whether pharmacological inhibitors could affect the invasion of organoids made from patient-derived xenograft (PDX) embedded into collagen-I gels. The organoids from CRC NOS adenocarcinoma form glandular structures characterized by cohesive cells (highlighted by E-cadherin staining) and apico-basolateral polarity (highlighted by the central lumen, Fig 4A) as previously described (Sato & Clevers, 2013). While in basal conditions, only $7 \pm 1\%$ of these organoids harboured protrusions, treatment with Y27632 and H1152 increased the number of protrusive structures to $78 \pm 4.6\%$ and $93 \pm 2.2\%$, respectively (Fig 4A and B). Next, we treated explants freshly retrieved from CRC patients with ROCK inhibitors. As described above, primary specimens were collected from patients (Fig EV2A) at the time of surgery and embedded into ECM gels. Treatment with these inhibitors did not affect the epithelial architecture of the CRC explants as shown by the presence of luminal cavities (Fig 4C, D and F and Movie EV3). Strikingly, Y27632 and H1152 triggered protrusions formation, increasing the number of invasive structures from $14 \pm 4\%$ to $63 \pm 6\%$ and $57 \pm 5\%$, respectively (Fig 4E and F and Movie EV3). We observed similar phenotypes from explants

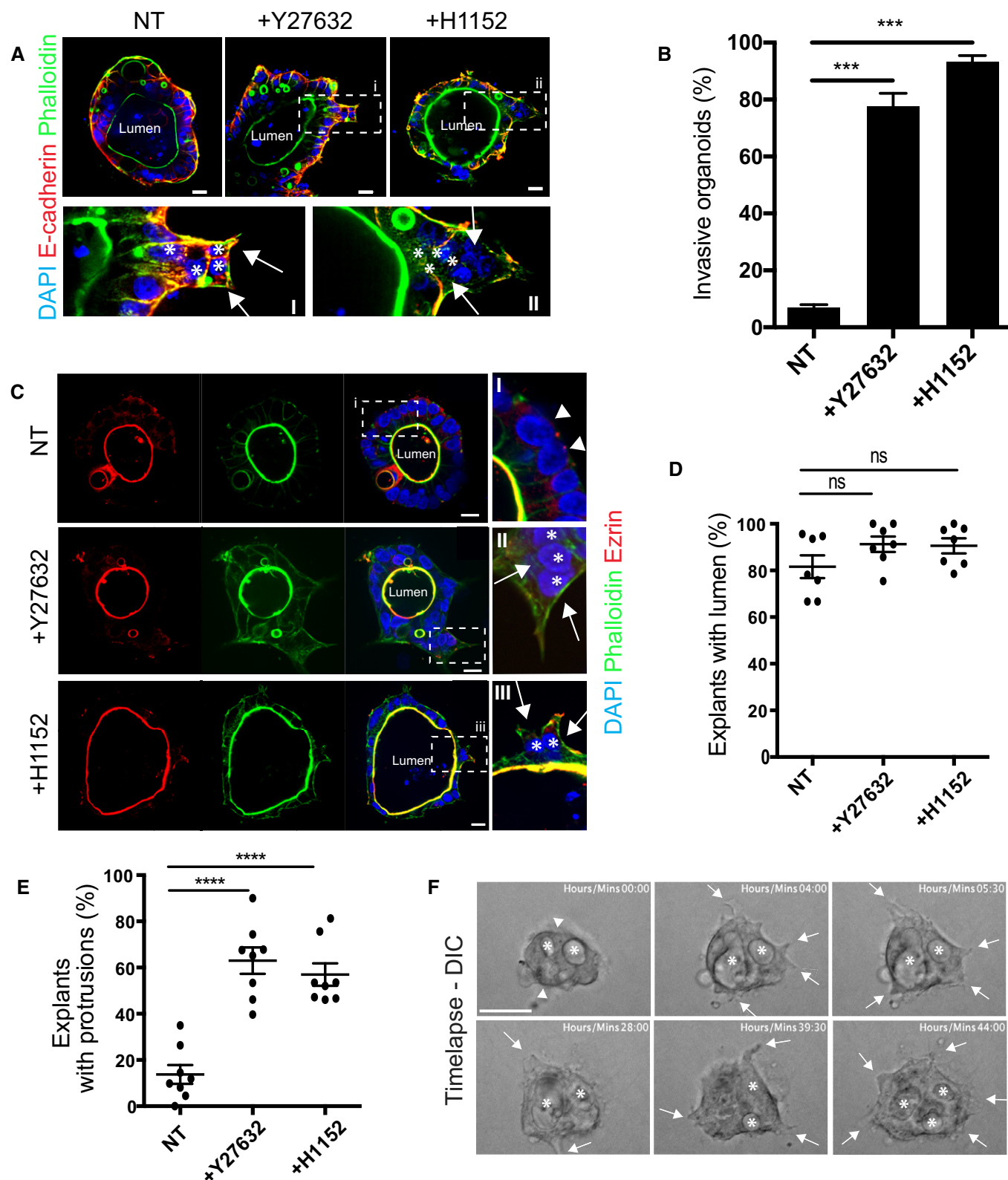


Figure 4.

retrieved from primary tumours or metastases (not shown), and the invasion capacities were not associated with KRAS mutations status (Fig EV2A). Altogether, our results demonstrate that the inhibition

of ROCK activity triggers the protrusive activity of NOS adenocarcinoma explants, organoids and cell lines to induce their collective invasion.

Figure 4. ROCK inhibition promotes the collective invasion of colorectal adenocarcinoma explants.

- A Representative images of organoids formed from patient-derived xenografts (PDXs) that have been embedded in collagen-I gels during 3 days, in non-treated (NT) or ROCK inhibitors-treated conditions (+Y27632) and (+H1152). At end point, organoids were stained for E-cadherin, F-actin (Phalloidin) and nuclei (DAPI). i and ii are high magnification of boxed regions of +Y27632 and +H1152 organoids, respectively. Arrows point to protruding cells. White stars show nuclei that engage in protrusions. Scale bars: 20 μ m.
- B The bar graph represents the percentage of protrusive organoids resulting from three independent experiments. Over 50 organoids were counted per condition (means \pm SEM). *P* values were calculated using paired *t*-test ($***P < 0.001$).
- C Representative images of human adenocarcinoma explants after 2 days in 3D collagen-I gel, in non-treated (NT) or ROCK inhibitors-treated conditions (+Y27632) and (+H1152) and stained for the apical pole (ezrin), F-actin (Phalloidin) and nuclei (DAPI). Boxed regions of NT, +Y27632 and +H1152 explants are shown at high magnification. Arrowheads point to non-protruding cells. Arrows point to protruding cells. White stars show nuclei that engage in protrusions. Scale bars: 20 μ m.
- D, E Explants displaying (D) lumens or (E) protrusive cells from 10 patients were quantified and results presented as percentage of total explants. Over 50 explants were counted per condition (duplicate) and per patient (means \pm SEM). *P* values were calculated using unpaired *t*-test ($****P < 0.0001$, n.s.: non-significant).
- F Time-lapse sequences of an adenocarcinoma explant undergoing collective invasion into collagen-I gel in the presence of Y27632 monitored by DIC microscopy for 2 days (corresponding to Movie EV3). Arrowheads point to non-protruding cells, arrows point to protruding cells, and white stars point to lumens. Scale bars: 50 μ m.

ROCK2 inhibition is sufficient to induce collective invasion

To differentiate the respective contribution of ROCK1 and ROCK2, we separately silenced the kinases in Caco-2 cysts and assessed for invasion (Fig EV3A). The depletion of ROCK1 did not increase the formation of protruding leader cells. In contrast, depletion of ROCK2 triggered the formation of invasive cysts, increasing from $6 \pm 1\%$ to $53 \pm 6\%$, equivalent to the co-depletion of both kinases and the treatment with Y27632 (Fig 5A and B). To investigate the role of ROCK2 kinase activity in collective invasion, we generated dominant negative mutants (DN), ROCK2DN#1 and ROCK2DN#2, as previously described (Amano *et al*, 1999). They correspond to the carboxy-terminal region of ROCK2 which includes the Rho binding (RB) and the Pleckstrin homology (PH) domains. Both constructs are predicted to bind ROCK2 catalytic domain, thereby competing with its substrates (and the ROCK2DN#2 harbours a point mutation in the RB domain to prevent the titration of RhoA-GTP). We tested their ability to interact with endogenous ROCK proteins in our Caco-2 cells. Protein complexes were immunoprecipitated using GFP-trap[®] beads from lysates expressing GFP-tagged ROCK2 DN constructs. Western blot revealed that GFP-ROCK2DNs interact with endogenous ROCK2, but not ROCK1 (Fig EV3E). When stably expressed in Caco-2 cells, ROCK2DN#1 perturbed Caco-2 cyst morphogenesis (as expected if it titrates RhoA-GTP) but mutation of the RB domain in ROCK2DN#2 allowed the formation of normal cysts with a single central lumen (Fig EV3F). We therefore only used the stable cell line expressing ROCK2DN#2 in our invasion assay. Expression of this construct increased the protrusion rate of Caco-2 cysts from $11 \pm 1\%$ to $51 \pm 1\%$ (Fig 5C and D). Then, to address whether ROCK2 activity was sufficient to restrain migratory behaviours, we used the T84 cysts that provides a pro-invasive model of colorectal adenocarcinoma. T84 cysts display a glandular organization with over 60% of them undergoing spontaneous collective invasion at steady-state or after transduction with GFP (Fig 5E and F). Treatment by Y27632 further increased T84 invasive cysts to $93 \pm 3\%$. Conversely, expression of dominant active ROCK2 (ROCK2-DA), corresponding to the catalytic domain of the kinase, reduces the number of protruding T84 cysts to $35.8 \pm 9\%$ (Fig 5E and F). Finally, to evaluate the clinical significance of our findings, we examined the correlation between the level of ROCK2 or ROCK1 mRNA and the survival of CRC patients using Kaplan–Meier analysis. Decreased level of ROCK2 expression (from two independent probes), but not ROCK1, significantly correlated with shorter overall patient survival (Fig 5G). Taken together, these

results demonstrate that ROCK2 activity prevents collective invasion from colorectal adenocarcinoma *ex vivo* and its decreased expression is correlated with poor patient prognosis.

ROCK2 inhibition promotes leader cell formation

We then investigated the mechanism of ROCK function. Inhibition of the kinase activity triggers the supracellular polarization of Caco-2 cysts resulting in the appearance of protrusive leader cells and non-protrusive followers. We reasoned that ROCK2 inhibition could either directly induce the formation of leaders or followers, or, alternatively, unleash cysts that include cells with a pre-existing leader fate. To examine this, we generated mosaic cysts to inhibit ROCK2 activity in a small subset of cells (Fig 6A). Mature Caco-2 cysts were transduced using a sub-optimal concentration of lentiviral particles encoding GFP-ROCK2DNs in order to target only 1 or 2 cells per cyst. Strikingly, the acute mosaic expression of ROCK2DN#2 increased the invasion to 74% (Fig 6B and C). We then measured whether ROCK2DN#2 expressing cells become leaders or followers. In control cysts treated with Y27632, $34.6 \pm 5.5\%$ of cells expressing GFP became leader cells. In contrast, $79.9 \pm 3.9\%$ of cells expressing ROCK2DN#2 were protrusive leaders (Fig 6D).

In other model systems, the small GTPases Rac1 controls F-actin polymerization in leader cells (Wang *et al*, 2010; Yamaguchi *et al*, 2015). We therefore reasoned that Rac1 could participate in leader cell formation in CRCs. To verify this hypothesis, we first used the CRIB domain of PAK to pull-down GTP-bound Rac1 in cell treated with the ROCK inhibitors. Western blot analyses revealed an increase in the level of Rac1-GTP after the treatment by Y27632 and H1152, with a few hours shift in the kinetic (12 and 16 h, respectively, Fig 6E). Then, we co-treated Caco-2 cysts with Y27632 or H1152 and the Rac inhibitor NSC23766 during our organotypic invasion assay. The treatment with NSC23766 decreased the number of protrusive cysts induced by Y27632 or H1152 treatment from $32 \pm 1\%$ to $14 \pm 4\%$ and $8 \pm 1\%$, respectively (Fig 6F and G).

These results demonstrate that there is not leader cell fate pre-determination in Caco-2 cysts and the inhibition of ROCK2 activity is sufficient to promote the formation of protrusive leaders downstream of Rac1 activation.

Caco-2 cyst invasion relies on FARP2 a GEF for Rac1

We then aimed at identifying the effectors of ROCK2 involved in Caco-2 cysts collective invasion. To identify the GEF mediating the

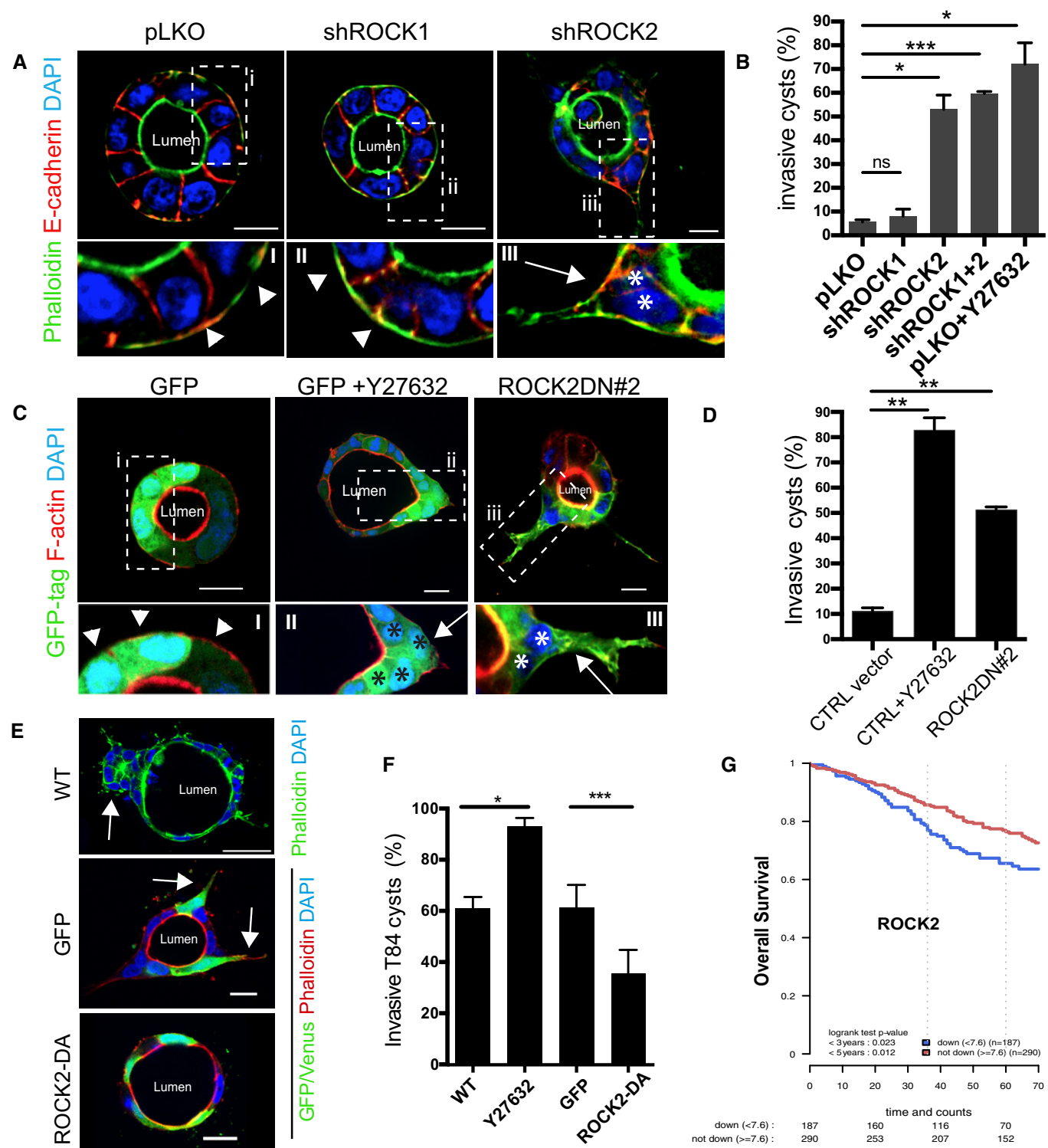


Figure 5.

activation of Rac1 downstream of ROCK inhibition, we used a siRNA-based screen in the adapted Boyden chamber assay (Fig 3D). For this, we transfected Caco-2 cells with a siRNA library targeting all known GEFs of the human genome and assessed collective invasion induced by Y27632. To prevent any functional redundancy, we grouped the siRNA targeting the two closest

homologs (Table EV2). The screen yielded 3 hits decreasing the invasion rate by threefold or more (Fig 7A). Two of the hits, targeting GEFs for RhoA and RhoG, were not confirmed in the validation round. The third hit, combining siRNA against FARP1 and FARP2, two GEFs for Rac1 and Cdc42, decreased by 3.8 ± 0.1 -fold the rate of invasion induced by Y27632 (Fig 7A,

Figure 5. ROCK2 inhibition is necessary and sufficient to control collective invasion.

- A Caco-2 cysts expressing an empty vector (pLKO) or shROCK1 (#02) or shROCK2 (#36) after 2 days of invasion were fixed and stained for E-cadherin, F-actin (Phalloidin) and nuclei (DAPI). Boxed regions i, ii and iii are shown at high magnifications. Arrowheads point to non-protruding cells. Arrow points to protruding cells. White stars show nuclei that engage in protrusions. Scale bars: 20 μ m.
- B The number of protrusive Caco-2 cysts was quantified in each of the mentioned conditions and represented in a bar graph as percentage of total cysts (means \pm SEM of at least 3 independent experiments, paired t-test, *** P < 0.001, * P < 0.05 n.s.: non-significant).
- C Caco-2 cysts stably expressing GFP alone or GFP-ROCK2DN#2 were submitted to a 2 days period invasion assay, then fixed and stained for F-actin (Phalloidin) and nuclei (DAPI). Boxed regions i, ii and iii are shown at high magnification. Arrowheads point to non-protruding cells. Arrows point to protruding cells. White and black stars show nuclei that engage in protrusions. Scale bars: 20 μ m.
- D Bar graph representing the percentage of protrusive cysts transduced with GFP (CTRL, with or without Y27632) or with ROCK2DN#2 (means \pm SEM of at least 3 independent experiments, paired t-test, ** P < 0.01 n.s.: non-significant).
- E T84 cells grown in 3D organotypic culture form polarized cysts with a central lumen that display protruding leader cells at the basal pole (arrows) reminiscent of collective invasion. T84 cysts were transduced with lentiviruses encoding inducible GFP or Venus-ROCK2-DA and treated with doxycycline 1 μ g/ml. Scale bars: 20 μ m.
- F Bar graph representing the percentage of protrusive T84 cysts in control (WT), treated with ROCK inhibitor (Y27632) or transduced with lentiviruses expressing GFP or Venus-ROCK2-DA after induction by doxycycline (means \pm SEM of at least 3 independent experiments) (paired t-test, *** P < 0.001, * P < 0.05).
- G Overall survival prognostic value of ROCK2 expression in colon cancer patients of the GSE33582 data set (n = 477 patients with survival annotation) using Kaplan–Meier survival analysis. The patient cohort was divided into tumours with or without a down-regulation of ROCK2 relatively to non-tumoural tissues (expression cut-off value corresponds to the 1st decile of ROCK2 expression in non-tumoural sample, i.e., 7.6). Log-rank test P -values for survival distribution difference are indicated at 3 and 5 years.

Pair#24) (He *et al*, 2013). To confirm these results and determine whether both FARP homologs participate in collective invasion, we independently depleted FARP1 or FARP2 using specific shRNAs and verified this did not perturb Caco-2 cystogenesis (Fig EV4A and B). Silencing FARP2 using two independent hairpins reduced the number of protruding Caco-2 cysts induced by Y27632 from $58 \pm 6\%$ to $25 \pm 6\%$ and $32 \pm 4\%$, respectively, while FARP1 depletion had no effect (Fig 7B and C). Depleting FARP2 in the pro-invasive T84 cysts reduced protrusion formation from $51 \pm 7\%$ to $33 \pm 7\%$ and $39 \pm 9\%$, respectively, confirming that this pathway is conserved across colorectal adenocarcinomas models (Fig EV4C). We confirmed that FARP2 is a GEF for Rac1 using GST-PAK pull-down after overexpression or shRNAs treatment and showed its activity is inhibited by the NSC23766 (Figs EV4D and 4E). Then, we asked how ROCK was regulating FARP2 activity. We could not co-immunoprecipitate overexpressed ROCK2 and FARP2 constructs or detect by Western blot any band shift suggestive of phosphorylation, implying that FARP2 is not a ROCK2 substrate (Data not shown). In support to this, FARP2 is not part of the ROCK substrate candidates identified by proteomic analyses (Amano *et al*, 2015). Instead, ROCK2 could indirectly regulate FARP2 by controlling its localization. To test this hypothesis, we examined the subcellular distribution of the proteins in Caco-2 by immunofluorescence. Endogenous ROCK2 localizes in the nucleus and at the apical junctional complex (AJC), while GFP-FARP2 associates with the basolateral membrane but is largely excluded from the AJC (Fig EV5A, top row). To evaluate whether ROCK activity could affect FARP2 recruitment at the AJC, we expressed GFP-FARP2-FL protein in 2D Caco-2 cells and treated with Y27632 or H1152. Both ROCK inhibitors promoted GFP-FARP2 recruitment at the AJC (stained with ZO-1 antibodies), which could be visualized by linescan measurement (Fig 7D and E). Quantitative analyses demonstrated that the FARP2/ZO-1 fluorescence intensity ratio increases by 23 and 32% after treatment with Y27632 and H1152, respectively (Fig 7F).

Taken together, the results support that the GEF FARP2 is a downstream effector of ROCK2 necessary for the collective invasion of Caco-2 cysts. ROCK2 does not directly phosphorylate FARP2; however, it prevents its localization at the AJC.

FARP2 activation and Myosin-II inhibition cooperate to induce collective invasion downstream of ROCK2 inhibition

Finally, we examined whether FARP2 was sufficient to induce collective invasion in Caco-2 cysts. Intriguingly, overexpressing GFP-tagged FARP2-FL did not induce the formation of protrusions (Fig 8A and B). Since FARP2-FL may be folded in an inactive conformation, we generated activated mutants harbouring point mutations on residues 730 and 733 (FARP2-Mut), a truncation of the PH2 domain (FARP2-del) or both (FARP2-del/Mut, Fig EV5B) (He *et al*, 2013). We could not detect any significant changes in the cysts expressing FARP2 activated mutants as compared with the cysts overexpressing FARP2-FL or GFP alone (Fig 8A and B). Since FARP2 activation was not sufficient to induce protrusive activity, we hypothesized that another effector of ROCK2 could participate in the regulation of collective invasion. To address whether Myosin-II was involved, we first inhibited the motor activity of Myosin-II by treating Caco-2 cysts with blebbistatin. Some cells formed long and thin F-actin-rich elongations resembling dendrites. This “dendritic” phenotype was very different from the broad protrusions produced by leader cells under ROCK2 inhibition, and we did not detect any engagement of the nuclei towards this structure (Fig 8C and D). We then used siRNAs to assess whether other functions of Myosin-II, such as the F-actin cross-linking activity (Vicente-Manzanares *et al*, 2009), could participate in the regulation of collective invasion. The depletion of Myosin-IIA, but not Myosin-IIB, reproduced the phenotype induced by blebbistatin but failed to induce leader cell formation (Fig 8C and D and EV5C). We finally checked whether Myosin-II and FARP2 could cooperate, downstream of ROCK, to control collective invasion. We performed a dose–response experiment to identify the sub-optimal concentration of blebbistatin that did not induce the “dendritic” phenotype (Fig EV5D). We further combined blebbistatin at this concentration with the expression of FARP2 constructs and assessed for protrusion formation. Expressing FARP2-FL or the activated mutants of FARP2 in combination with 10 μ M of blebbistatin increased the formation of invasive cysts from $13 \pm 6\%$ to $59 \pm 6\%$, $50 \pm 14\%$ and $45 \pm 6\%$, respectively (Fig 8E and F). Thus, FARP2 can induce the formation of leader cells solely when the acto-myosin cytoskeleton is relaxed.

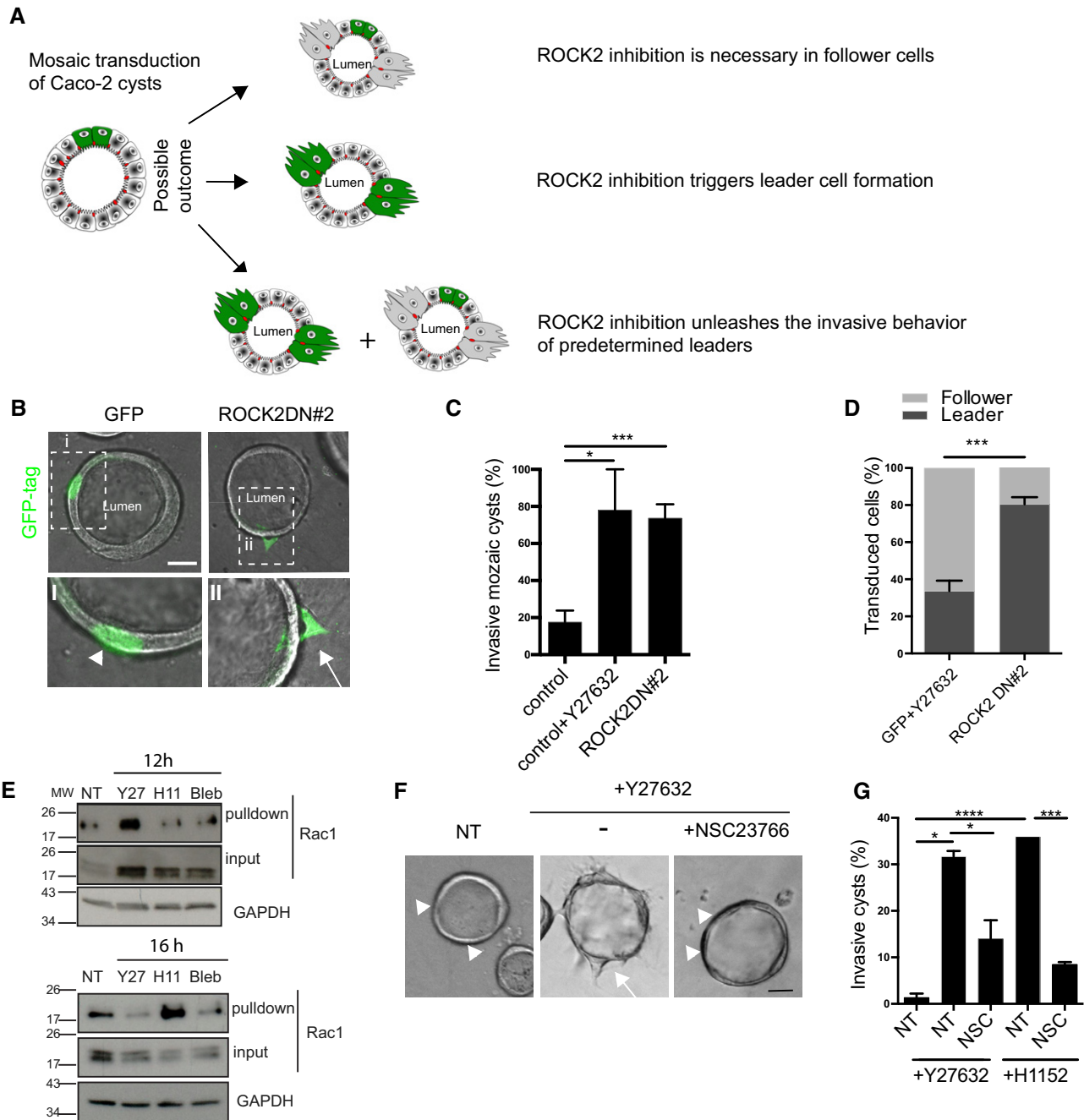


Figure 6. ROCK2 inhibition promotes leader cell formation.

- A Schematic representation of Caco-2 cyst phenotypes obtained after mosaic transduction of ROCK2DN#2.
- B DIC acquisition of fixed mosaic Caco-2 cysts expressing GFP alone, GFP-ROCK2DN#1 or GFP-ROCK2DN#2. Boxed regions i and ii are shown at high magnification. Arrowheads point to non-protruding cells. Arrows point to protruding cells. Scale bars: 20 μ m.
- C Bar graph representing the percentage of mosaic Caco-2 cysts transduced with GFP or GFP-ROCK2DN#, with or without Y27632, harbouring a protruding morphology (means \pm SEM of at least 3 independent experiments, unpaired *t*-test, ****P* < 0.001, **P* < 0.05).
- D Quantification of the fate of the GFP-positive cells, leader or follower, in mosaic cysts transduced with GFP alone and treated with Y27632 (GFP+Y27632) or GFP-ROCK2DN#2 from 3 independent experiments (means \pm SEM, unpaired *t*-test, ****P* < 0.001).
- E Representative pull-down of Rac1-GTP by PAK-Crib, in Caco-2 cells treated with ROCK inhibitor Y27632, H1152 or blebbistatin and lysed at 12 or 16 h. Immunoblot analyses were performed with anti-Rac1 and anti-GAPDH antibodies from three independent experiments.
- F DIC acquisition of fixed Caco-2 cysts treated with ROCK inhibitors alone (Y27632 or H1152), or in combination with Rac1 inhibitor NSC23766. Arrowheads point to non-protruding cells, and arrow points to protruding cell. Scale bar 20 μ m.
- G Bar graph representing the percentage of protruding Caco-2 cysts in control conditions (non-treated, NT) or treated with NSC23766, Y27632 or H1152 (means \pm SEM of at least 3 independent experiments, unpaired *t*-test, *****P* < 0.0001, ****P* < 0.001, **P* < 0.05).

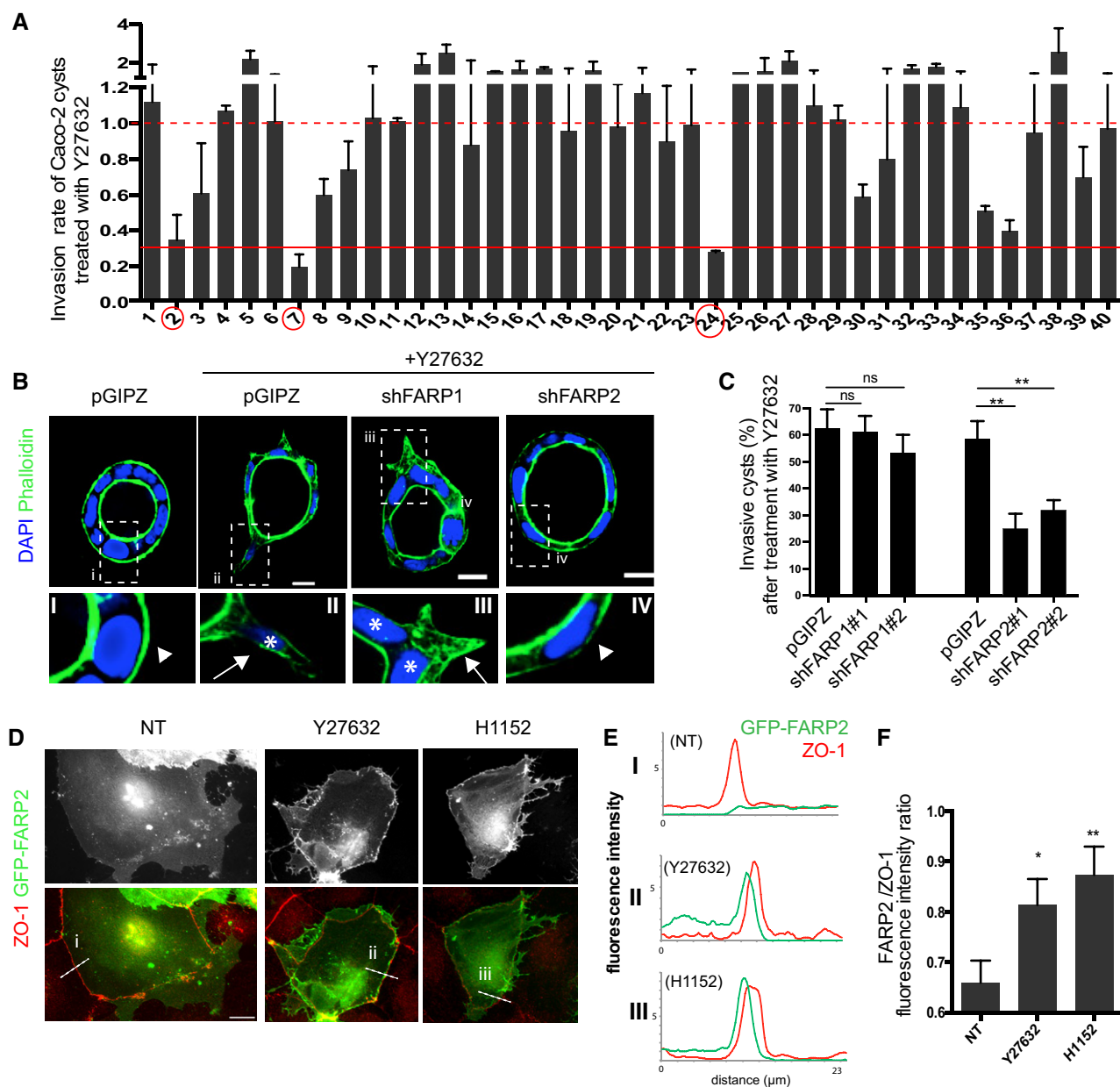


Figure 7. Caco-2 cysts collective invasion relies on the Rac-GEF FARP2.

- A** siRNA screen performed in Caco-2 cysts treated with Y27632: Caco-2 cells transfected with control siRNA or siRNA targeting RhoGEFs were seeded in the modified 3D Boyden chamber (Fig 3D) and grown as cysts for 3 days. Then, Caco-2 cysts were treated with Y27632, and the serum gradient was induced. After 2 days, the number of cells present on the bottom chamber was quantified by automated segmentation after Hoechst staining. The bar graph represents the mean invasion rate. Each condition was duplicated. The red dashed line represents the median invasion rate; the red full line indicates the threefold decrease in invasion rate. Three hits were identified: #2: ARHGEF18+RNEF, #7: SGEF+ARHGEF16 and #24: FARP1+FARP2 (mean \pm SD).
- B** Caco-2 cysts stably expressing empty vector (pGIPZ) or 2 distinct shFARP1 or shFARP2 were treated with Y27632, allowed to invade for 2 days, fixed and stained for F-actin (Phalloidin). Boxed regions i, ii, iii and iv are shown at high magnification. Arrowheads point to non-protruding cells; arrows point to protruding cells. White stars show nuclei that engage in protrusions. Scale bars: 20 μm .
- C** Bar graphs representing the percentage of protrusive cysts formed from Caco-2 cells transduced with lentiviruses encoding pGIPZ or shRNA against FARP1 and FARP2 after treatment with Y27632 from at least 3 independent experiments (means \pm SEM, paired t-test, ns: non-significant, ** P < 0.01).
- D** Representative acquisition of Caco-2 cells overexpressing GFP-FARP2 grown in 2D and stained with ZO-1, in non-treated condition (NT) or after 2 h with Y27632 or H1152. The dashed lines crossing the cell–cell junctions (i, ii and iii) are representative of the linescans measurements. Scale bars: 20 μm .
- E** Representative fluorescence intensity of ZO-1 (red) staining and GFP-FARP2 (green) along the dashed line i, ii and iii represented in Fig 7D corresponding to non-treated, Y27632 or H1152 treatments.
- F** Bar graph representing the average ratio of GFP-FARP2 over ZO-1 fluorescence intensities measured with linescans crossing cell–cell junctions. The quantification was performed on 71 cells expressing GFP-FARP2-FL from three independent experiments. For each cell, between 10 and 15 lines (12 pixels wide) were drawn across random region of cell–cell junctions positive for ZO-1 staining (mean \pm SEM unpaired t-test ** P < 0.01, * P < 0.05).

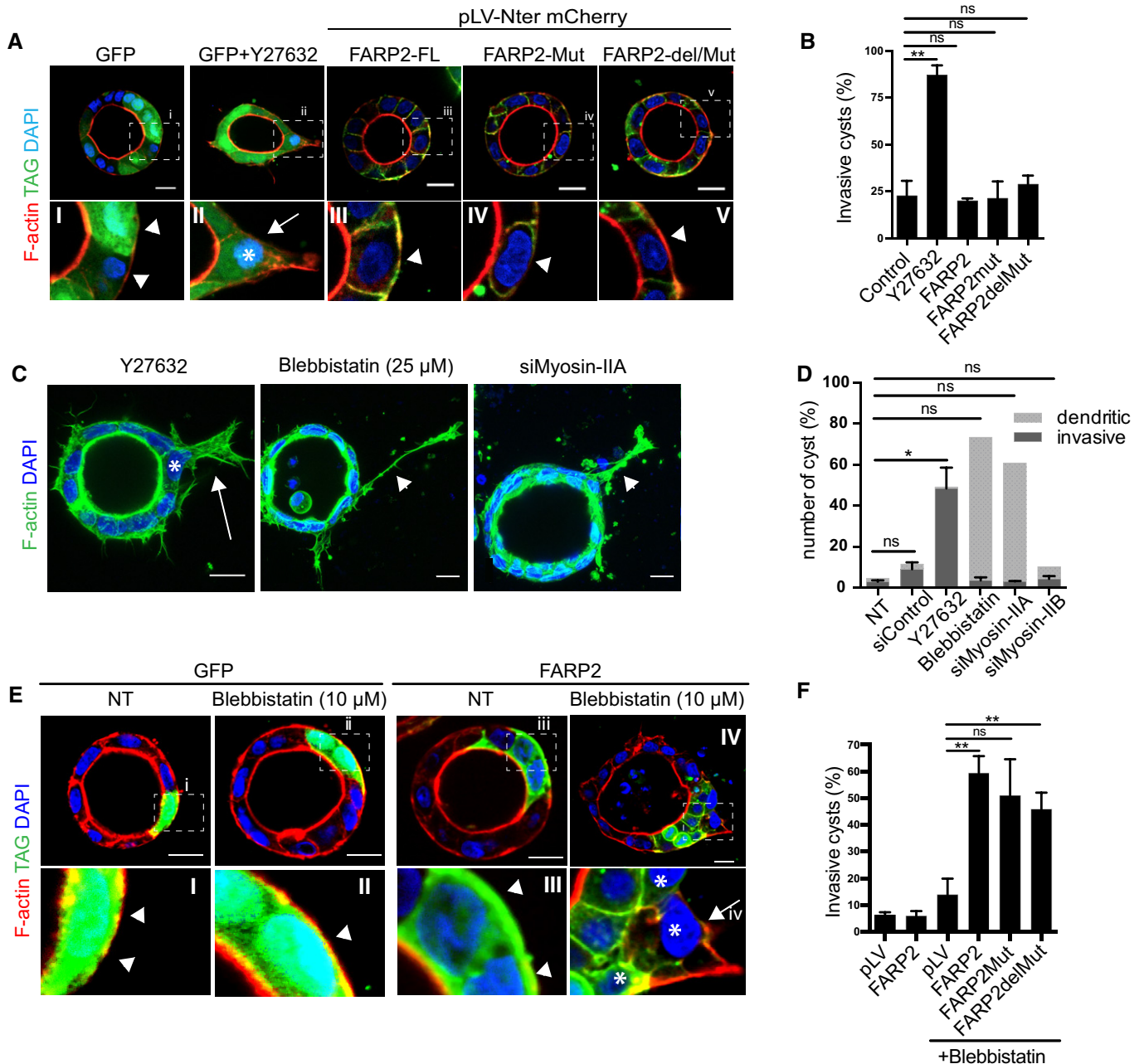


Figure 8. FARP2 activation and Myosin-II inhibition cooperate to induce collective invasion downstream of ROCK2 inhibition.

- A** Caco-2 cysts stably expressing GFP (treated or not with Y27632), or cherry-FARP2-full length (FARP2-FL), FARP2-730/733 mutant (FARP2-Mut) or FARP2 del PH 730/733 (FARP2-del/Mut) were allowed to invade for 2 days, fixed and stained for F-actin. Boxed regions i, ii, iii, iv and v are shown at high magnification. Arrowheads point to non-protruding cells, arrow points to protruding cells, and white star shows nucleus that engages in protrusion. Scale bars: 20 μ m.
- B** Bar graph representing the percentage of protrusive cysts expressing GFP (treated or not with Y27632) or the mentioned GFP-FARP2 constructs from 3 independent experiments (means \pm SEM, paired *t*-test, $^{**}P < 0.01$, n.s.: non-significant).
- C** Representative images of Caco-2 cysts treated with Y27632 or blebbistatin or transfected with siRNA targeting Myosin-IIA and allowed to invade for 2 days. After fixation, the cysts were stained for F-actin (Phalloidin) and nuclei (DAPI). Representative Y27632-induced "invasive" phenotype and blebbistatin-induced "dendritic" phenotype are displayed. Arrow points to protruding cells, white star shows nucleus that engages in protrusion, and arrowheads point to "dendritic" protrusions.
- D** Bar graph representing the percentage of cysts with the "invasive" or "dendritic" phenotypes after treatment with Y27632, blebbistatin or siMyosin-IIA or siMyosin-IIIB from at least 3 independent experiments (means \pm SEM, unpaired *t*-test, $^{*}P < 0.05$, n.s.: non-significant).
- E** Mature Caco-2 cysts were transfected with GFP or cherry tagged FARP2-full length (FARP2-FL), FARP2-730/733 mutant (FARP2-Mut) or FARP2 del PH/730/733 (FARP2-del/Mut), and treated (or not, NT) with blebbistatin. 2 days after invasion, and the cysts were fixed and stained for F-actin. Boxed regions i, ii, iii and iv are shown at high magnification. Arrowheads point to non-protruding cells; arrow points to protruding cells; and white stars show nuclei that engage in protrusions. Scale bars: 20 μ m.
- F** Bar graph representing the percentage of protrusive Caco2 cysts expressing the mentioned constructs, treated or not with blebbistatin, from at least 3 independent experiments (means \pm SEM, *t*-test, $^{**}P < 0.01$, n.s.: non-significant).

Altogether, these results demonstrate that FARP2 activation and Myosin-II inhibition cooperate downstream of ROCK2 to regulate the collective invasion of colorectal adenocarcinoma models.

Discussion

Enabling invasive properties is the first step of the metastatic cascade and a challenge to patient treatment. Based on the analyses of fixed and live cancer explants, this study revealed that NOS CRC, the most common type of CRCs representing about 80% of these cancers, maintains their epithelial glandular architecture while undergoing collective invasion to conquer the successive layers of the digestive wall. We identified ROCK2 as an essential kinase controlling the invasive behaviour of CRCs models such as cysts and organoids. ROCK2 inhibition triggers the formation of leader cells through a dual mechanism involving the reduction of Myosin-II activity and the activation of Rac1 through the GEF FARP2 to generate protrusive forces.

The analysis of CRC specimens collected from patients demonstrates that the tumour remains mainly cohesive through E-cadherin-based junctions while invading the submucosa or 3D collagen-I gels. This is consistent with the growing body of evidences supporting the contribution of collective behaviour to the metastatic spread of several cancer types, from patients or mice models, at early or late stages of cancer progression (Friedl *et al*, 1995, 2012; Giampieri *et al*, 2009; Cheung & Ewald, 2016; Khalil *et al*, 2017; Konen *et al*, 2017; Zajac *et al*, 2018). While in the past decades, most of the biomedical research investigations have focused on the EMT programme, seen as the main driver of cancer cell dissemination (Chaffer *et al*, 2016), this concept has recently been challenged by the demonstration that pancreas and breast cancer metastases form in mice without activation of the EMT transcription factors (Fischer *et al*, 2015; Zheng *et al*, 2015b) or that the EMT programme is in fact activated into the stromal component of CRCs (Kim & Verhaak, 2015). However, inhibiting EMT activation by silencing Zeb1 in CRC cell lines transplanted into immunodeficient mice decreases metastases formation (Spaderna *et al*, 2008; Wellner *et al*, 2009). These discrepancies could be explained by inter- and intra-tumoral heterogeneity or cancer cell plasticity and imply that dissemination strategies can be multiple and possibly complementary (Friedl & Alexander, 2011).

Surprisingly, we found that CRCs NOS/adenocarcinoma primary samples, organoids and cysts retain their epithelial polarity and architecture, invading as glandular structures *in vivo*, into the peritumoral stroma, or *in vitro*, in collagen-I gel. This is consistent with the fact that 80% of CRCs are well to moderately well-differentiated tumours (Prall *et al*, 2009; Fleming *et al*, 2012). This is a distinctive feature among the collective invasion of cancer cells reported to date. The apico-basolateral polarity of transformed epithelial cells is either lost, such as in breast carcinoma, or inverted, such as in the Mucinous or micropapillary types of CRC (Khalil *et al*, 2017; Zajac *et al*, 2018). However, during normal development and organogenesis, epithelial cell cohorts undergo collective migration while maintaining central lumens. In this case, the lumen enables growth factors concentration or exosome transfer favouring the activation of tyrosine kinase receptors (Durdu *et al*, 2014; Kwon *et al*, 2014; Revenu *et al*, 2014). Whether the luminal cavity of CRC glands

provides a selective advantage for tumour dissemination or proliferation is an attracting area of investigation.

We found that inhibition of ROCK triggers the formation of leaders and the transition from non-invasive to protrusive cohorts that undergo collective invasion. This is in contradiction with the pro-invasive role of ROCK identified in CIMP CRCs explants (Zajac *et al*, 2018), mice xenografted with cell lines (Itoh *et al*, 1999; Croft *et al*, 2004; Sadok *et al*, 2015) or transgenic models of pancreatic cancer (Rath *et al*, 2018). However, our results are in agreement with the recent large-scale *in vivo* RNAi screen revealing that loss of Myosin-II triggers the formation of invasive skin cancers (Schramek *et al*, 2014) and that expression of active ROCK2 increases proliferation, but not invasion in similar models (Samuel *et al*, 2011). By investigating the early step of collective invasion, i.e., the transition from quiescent to invasive glands, we have revealed the anti-invasive activity of ROCK2, a function that may not have been identified from cancer cells that have already gained invasive capacities. Our results are supported by the study from Lomakin *et al* showing that Myosin and ROCK inhibition triggers the migratory behaviour of non-motile single epithelial cells (Lomakin *et al*, 2015). The discrepancies in the role of ROCK in invasion could also be related to several aspects of cancer heterogeneity. First, the histological type and/or the molecular background of cancer may influence invasion mode and ROCK function. In line with this, ROCK has an anti-invasive role in NOS CRCs that mostly display chromosomal instability, and a pro-invasive function in MUC CRCs that arise from the CIMP pathway of carcinogenesis (Zajac *et al*, 2018). In addition, crosstalk with specific oncogenes and tumour suppressors, such as KRAS, Smad4 or JAK1, can modify the expression level and activity of ROCK (Sahai *et al*, 2001; Hoogwater *et al*, 2010; Sanz-Moreno *et al*, 2011; Voorneveld *et al*, 2014), yet we did not detect a significant correlation with KRAS status in our cohort (Fig EV2A). Second, ROCK may have different actions if the tumour spreads as individual cells or collectives. In single cells, increased acto-myosin contractility would promote fast amoeboid invasion, likely accelerating metastases formation (Sahai & Marshall, 2003). In contrast, reducing cortical tension in cell cohorts, at cell-cell junctions or the basal membrane, would be beneficial for collective invasion (Fischer *et al*, 2009; Giampieri *et al*, 2009; Hidalgo-Carcedo *et al*, 2011). Third, the tissue in which the tumour is borne may influence ROCK function and elicit different responses to its inhibition. While interfering with ROCK and Myosin-II activity has long been known to impede fibroblast movement, recent work has demonstrated that it promotes the migration of single epithelial cells (Lomakin *et al*, 2015).

How does ROCK2 control the invasive behaviour of CRC neoplastic glands? Using the acute expression of dominant negative mutants, we targeted ROCK2 inhibition in a restricted number of cells within the cohort. This was sufficient to induce leader cell formation, demonstrating that unlike breast and lung carcinomas, CRC leaders are not predetermined by a transcriptional programme (Cheung *et al*, 2013; Konen *et al*, 2017). Nevertheless, the activation of specific gene expression may be induced downstream of ROCK inhibition by mechanosensing proteins such as YAP/TAZ or Stat3 (Dupont *et al*, 2011; Sanz-Moreno *et al*, 2011). We show that ROCK controls two distinct F-actin dynamics, F-actin polymerization through Rac1 and F-actin contractility through Myosin-II. Rac1 activation is a common determinant of leader cell formation (Wang *et al*, 2010; Yamaguchi *et al*, 2015). Yet, our screen targeting all

human GEFs did not identify β bix, Tiam1 or DOCK180 that have been previously described to activate Rac1 in collective migration (Osmani *et al*, 2006; Bianco *et al*, 2007; Ellenbroek *et al*, 2012). Although the ROCK/Rac1 balance is a core mechanism controlling all migratory processes, the GEFs and GAPs governing their spatiotemporal activation vary with cell types and stimuli (Sadok & Marshall, 2014). We found that FARP2 activity was necessary for Caco-2 collective invasion induced by ROCK inhibition, but not FARP1. While they both regulate cytoskeleton dynamics (Kubo *et al*, 2002; Toyofuku *et al*, 2005; Zhuang *et al*, 2009; Cheadle & Biederer, 2012, 2014; Mlechkovich *et al*, 2014), these two GEFs act downstream of distinct signalling pathways to control neurite outgrowth, axon collapse, podosome formation or bone metabolism (Koyano *et al*, 1997, 2001; Takegahara *et al*, 2010) and only FARP2 has been reported to regulate cell motility (Miyamoto *et al*, 2003).

While the photo-activation of Rac1 is sufficient to drive the collective migration of border cells, FARP2 expression is ineffective at triggering Caco-2 cyst collective invasion. Downstream of ROCK, we found that relaxing acto-myosin contractility is required to unleash collective invasion. This is in agreement with previous reports from 2D cultures, where breaking up the supracellular marginal actin bundle and loosening acto-myosin tension at cell–cell junctions both contribute to collective migration (Omelchenko *et al*, 2003; Hidalgo-Carcedo *et al*, 2011; Omelchenko & Hall, 2012; Refay *et al*, 2014). In addition, releasing actin bundles frees actin monomers increasing the pool of soluble G-actin necessary to fuel branched F-actin polymerization in protrusion as described by Lomakin *et al* in single epithelial cells (Lomakin *et al*, 2015).

Together, our results show that ROCK activity synchronizes the cytoskeleton to harness CRC invasive behaviour. ROCK inhibitors being already used in the clinic for the treatment of several cardiovascular conditions, it has been proposed to target ROCK in cancer patients to prevent or reduce invasion and metastasis formation (Croft *et al*, 2004; Narumiya *et al*, 2009; Sadok & Marshall, 2014; Vennin *et al*, 2017). Yet, it remains essential to account for cancer heterogeneity and elucidate the tumour specific context enabling pro or anti-invasive functions of this kinase in order to propose relevant therapeutic strategies to patients and avoid paradoxical effects.

Materials and Methods

Primary specimens from colorectal carcinoma patients

The human study protocols followed all relevant ethical regulations in accordance with the declaration of Helsinki principles. Tumour specimens were obtained after informed patient consent at Gustave Roussy Hospital.

Live cancer specimens

Primary tumour and metastasis explants were retrieved from CRC patients at the time of surgery. The freshly isolated samples were transferred to sterile tubes. DMEM containing 4.5 g/l glucose, glutaMAX (Life Technologies, 31966021) and 100 UI/ml penicillin, 100 μ g/ml streptomycin (1% P/S) (Life Technologies, 15140-122) was added to a final volume of 10 ml. The freshly isolated tumours were minced into small fragments and incubated under shaking conditions for 55 min to

1 h 15 at 37°C in a final volume of 1 to 5 ml of DMEM supplemented with 2 mg/ml of collagenase. Digested tumour clusters were filtered through a 100- μ m filter and pelleted for 5 min at 850 g. The pellet was resuspended in 10 ml of complete DMEM and pelleted for 10 s at 850 g, and finally, the resuspended pellet in 10 ml of complete DMEM was pelleted by 3–5 pulse centrifugations from 850 g to 425 g. The tumour fragments, free of single cells, were embedded in 100% Matrigel in a culture dish, and DMEM supplemented with 10% FBS was added on top. Culture was maintained 3 days for recovery. Then, explants were washed in DMEM, pelleted at 500 g and used for invasion assay.

Fixed cancer specimens

Primary CRC and metastases specimens obtained after surgical resection were formalin-fixed and paraffin-embedded (FFPE) according to hospital routine protocols. We selected NOS “Not Otherwise Specified” types of CRC (also called lieberkuhnian or adenocarcinoma in the World Health Organization classification). 3- μ m sections of FFPE samples were deparaffinised, unmasked (Ph8) and rehydrated prior haematoxylin–eosin–safran (HES) or Alcian blue staining, immunohistochemistry or immunofluorescence. For the specific view of the CRC invasion margin, the tumours were cut with one transverse incision to expose a full view of the invasion margin at its deepest point. From the invasion margins, several cubes of about 1 \times 1 \times 1 mm were immersion fixed in buffered glutaraldehyde (4%), blocked in epoxy resin and cut serially at 0.5 μ m thickness. A Movat’s stain was used for light microscopic study. For electron microscopy, the epoxy resin blocks were trimmed for visualization of areas with invasive neoplastic glands. 50-nm ultrathin sections were taken, mounted on copper grids (200 mesh) and contrasted with uranyl acetate and lead citrate.

Organoids from Patient-derived Xenograft (PDX)

Animal experiments were compliant with French legislation and EU Directive 2010/63. The project was validated by the Ethical Committee (CEEA) no. 26 and was then granted French government authorizations under number 517-2015042114005883. Mice were obtained from Charles River, housed and bred at the Gustave Roussy animal core facility (accreditation number E-94-076-11). Animals were humanely euthanized according to end points that were validated by the Ethical Committee and the French government (Ministère de l’Enseignement Supérieur, de la Recherche et de l’Innovation). The human colorectal tumour corresponding to LRB-0010P from the CREMEC tumour collection was maintained in NOD SCID Gamma (NSG from Charles River, France) mice as previously described by Julien *et al* (2012). Briefly, small tumour fragments were subcutaneously engrafted on the flank of anesthetized mice (2.5% isoflurane). Tumour growth was measured at least once a week. When the volume reached 1,000–1,500 mm³, mice were sacrificed and tumours were used for *ex vivo* experiments and 50-mm³ fragments engrafted on the flank of new mice. Organoids were prepared as described previously (Ewald *et al*, 2012). Tumours were minced into small fragments and were incubated for 1 h 30 at 37°C in a final volume of 5–10 ml of DMEM supplemented with 2 mg/ml of collagenase. Digested tumour clusters were pelleted by 4 pulse centrifugations at 1,500 rpm. The tumour fragments, free of single cells, were maintained 3 days in culture medium supplemented with 15% Matrigel to allow formation of polarized organoids. Then,

organoids were washed in DMEM, pelleted at 1500 rpm and used for invasion assay.

Cell lines and culture conditions

Colorectal carcinoma cell line Caco-2 and T84 were purchased at ATCC and grown in complete medium (DMEM/GlutaMAX for Caco2 and DMEM/F12 for T84), supplemented with 10% foetal bovine serum (FBS) and 1% P/S. Normal colon fibroblast cells, CCD-18CO (ATCC), were grown in Eagle's Minimum Essential Medium supplemented with 1% non-essential amino acids (NEAA) 10% FBS and 1% P/S and used at 70–80% confluence to produce conditioned media (harvested after 24 h and stored at -20°C until use). All cells were grown in a humidified atmosphere at a temperature of 37°C and with 5% CO_2 .

Caco-2 and T84 cyst morphogenesis

The following mix was used to coat the wells of 8-well Ibidi chamber (10 μl per well): Matrigel was mixed with Rat-tail Collagen-I neutralized with NaOH (1M), Hepes (1M) and MEM (10x) (Life Technologies, 21430-02) according to the ratio 0.843:0.025:0.032:0.1 (vol/vol/vol/vol), adjusted with DMEM 1X and allowed to polymerize in ice for 30 min before adding the Matrigel and coating the dish. Polymerization occurred within 30 min at room temperature. The final concentrations of the mix were 4.5 mg/ml for Matrigel and 1.3 mg/ml for Collagen-I. Caco-2 cells were dissociated into single cells with trypsin-EDTA and resuspended in ice-cold DMEM complete medium supplemented with Matrigel (2%), and cholera toxin (0.01 $\mu\text{g}/\text{ml}$) (DMEM-MG-CT). The cell suspension was then added on top of the coating (10⁵ cells per well). The morphogenesis proceeded for 3 days at 37°C to allow formation of Caco-2 cysts.

Invasion assays

Patient primary cancer specimens and organoids

Tumour explants and organoids were embedded in 2 mg/ml neutralized rat collagen-I and added on top of the pre-coated well at a concentration of 1–2 cluster per microlitre. The gel was allowed to polymerize for 45 min at 37°C . Culture medium supplemented with FBS (10%) was added to the wells, and invasion was allowed to proceed for up to 6 days. In fixed experiments, invasive explants and organoids were defined as the ones with strand of cells invading the 3D matrix led by protrusive cells at the front. At least 40 organoids and 50 explants were counted per condition.

Caco-2 and T84 cyst invasion assays

1/After morphogenesis, the complete medium supplemented with 2% Matrigel (+/– lentiviruses) was discarded, while the cysts remained adherent to the Matrigel/Collagen-I coating. Collagen-I at a final concentration of 1.3 mg/ml was added on top of the Caco-2 cysts and allowed to polymerize 15 min at room temperature. Then, CCD-18-CO cells conditioned medium supplemented with cholera toxin with or without inhibitors was added on top of the cysts. Caco-2 cysts were allowed to perform invasion for 2 days at 37°C . 2/The adapted Boyden chamber invasion assay: Caco-2 cyst morphogenesis

was allowed to proceed on the top chamber of the Boyden as follows: Matrigel mixed with ice-cold DMEM 1X to a final concentration of 4.5 mg/ml was used to coat the top side of the Boyden membrane (4 μl per membrane) and allowed to polymerize at 37°C for 10 min. Caco-2 cells were dissociated into single cells and resuspended in ice-cold DMEM with 2% Matrigel and cholera toxin. The cell suspension was then added on the top chamber and left to form cysts for 3 days at 37°C . Once the cysts were formed, a growth factor gradient was created by replacing the top's chamber complete medium with 2% Matrigel without FBS, whereas the bottom chamber was renewed with DMEM supplemented with FBS (10%). Caco-2 cells were allowed to invade towards the bottom chamber for 2 days.

The number of invaded cells was calculated using an automated segmentation analysis after nucleus staining (Hoechst) using the Metamorph “count nuclei” application.

Small molecules inhibitors

H1152 (Tocris, 2414), Y27632 (Calbiochem, 688000), blebbistatin (Calbiochem, 203391), NSC-23766 (Tocris, 2161) were used at 2 μM , 25 μM , 10 to 25 μM and 200 μM , respectively, doxycycline (Sigma-Aldrich, D9891) was used at 1 $\mu\text{g}/\text{ml}$.

SiRNA transfection

siRNA oligonucleotides on-target smart pools targeting Rho-GTPases effectors and GEFs were purchased from Dharmacon™. The complete list of genes and corresponding catalogue numbers is provided in Tables EV1 and EV2. siRNA (100 nM) were transfected into Caco-2 cells using Dharmafect 1 Transfection Reagent (Dharmacon™, T-2001, 1:57) diluted in Opti-MEM medium (Gibco, 31985070). Briefly, Caco-2 cells were plated in culture dish in complete medium, the day after the medium was replaced with complete medium without antibiotics and the siRNA/Dharmafect mix (1:5) was added to the medium. After 6 h, the transfection medium was replaced with complete medium. The cells were allowed to recover overnight before embedding into 3D matrices (the effector screen was performed in Caco-2 cysts cultivated in 3D Matrigel and collagen-I. The GEFs screen was carried out in the 3D Boyden Chamber assay).

shRNAs reagents

ROCK shRNAs were provided in a pLKO.1 expression vector and were purchased from Sigma; shRNA ROCK1 (TRCN0000195202) shRNA ROCK2 (TRCN0000194836). shRNAs targeting FARP1 and FARP2 were purchased from ThermoFisher and provided in a pGIPZ expression vector; FARP1#1 (V3LHS_325427), FARP1 #2 (V3LHS_325430), FARP2#1 (V2LHS_95483), FARP2#2 (V3LHS_369923), FARP2#3 (V2LHS_369924), FARP2#4 (V2LHS_369925). All vectors encoding shRNAs were transduced using lentiviruses (see below).

Expression vector

The Tet-inducible dominant active Rock2 lentivirus construct (Rock2-DA) was provided by Sanjay Kumar (Addgene pSlik-Rock2: 84649).

Expression vectors (Gateway cloning system)

cDNAs of FARP1-FL, FARP2-FL, FARP2-Mut, FARP2-del and FARP2-del/Mut, provided by Pr. Zhang (He *et al*, 2013), were cloned into lentiviral expression vectors pLV-Nter cherry and ROCK2DN#1; ROCK2DN#2 cDNAs were cloned into lentiviral expression vectors pLV-Nter-GFP using the Gateway recombination cloning system. To generate the entry clones (pDONR221), all cDNAs were obtained by polymerase chain reaction (PCR) using the Phusion High-fidelity Taq DNA polymerase (NEB, M0530) according to the manufacturer instructions. pDONR221-ROCK2DN#2 was generated using oligonucleotide-directed PCR mutagenesis to create an Asn to Thr and a Lys to Thr replacement at amino acids 1036 and 1037, respectively, from pDONR221-ROCK2DN#1. The following primers were used:

Lentiviruses transduction

Virus production

The shFARP1#1 and #2, shFARP2#1 and #2, shROCK1#02, shROCK2#36, ROCK2DN#1, ROCK2DN#2, FARP1, FARP2-FL, FARP2Mut, FARP2delMut lentiviral particles were obtained by transfecting the respective expression lentiviral vectors with the packaging vectors pMD2G (Addgene, 12259) and pCMVdR8.74 (Addgene, 22036) into HEK293T (ATCC) cells with the transfection reagent JetPrime (Polyplus, 114-15, 1:250) diluted in the JetPrime buffer (Polyplus, 712.60). Lentiviruses-containing supernatants were collected on days 2 and 3 following transfection and were concentrated by ultracentrifugation (24,500 g, 2 h) and then stored at -80°C .

Construct name	Primer name	Primer sequence	Template
pDONR-FARP1-FL	F1STARTMET-For	5' GGGG ACA AGT TTG TAC AAA AAA GCA GGC TTC <u>ATG</u> GGA GAA ATA GAG CAG AGG 3'	pCDNA3.1+FARP1-FL nter flag (human)
	F1ENDSTOP-Rev	5' GGG GAC CAC TTT GTA CAA GAA AGC TGG GTC <u>TCA</u> ATA CAC AAG AGA CTC TTT GTG 3'	
pDONR-FARP2-FL	F2STARTMET-For	5' GGGG ACA AGT TTG TAC AAA AAA GCA GGC TTC <u>ATG</u> GGA GAG ATA GAA GGA ACA TAC 3'	pCDNA3.1+FARP2-FL nter flag (mouse)
	F2ENDSTOP-Rev	5' GGGG AC CAC TTT GTA CAA GAA AGC TGG GTC <u>TCA</u> GAG GTT CTT GTC CAA GCAGGGT 3'	
pDONR-FARP2-Mut	F2STARTMET-For	5' GGGG ACA AGT TTG TAC AAA AAA GCA GGC TTC <u>ATG</u> GGA GAG ATA GAA GGA ACA TAC 3'	pCDNA3.1+FARP2-Mut nter flag (mouse)
	F2ENDSTOP-Rev	5' GGGG AC CAC TTT GTA CAA GAA AGC TGG GTC <u>TCA</u> GAG GTT CTT GTC CAA GCAGGGT 3'	
pDONR-FARP2-Del	F2STARTMET-For	5' GGGG ACA AGT TTG TAC AAA AAA GCA GGC TTC <u>ATG</u> GGA GAG ATA GAA GGA ACA TAC 3'	pCDNA3.1+FARP2-del nter flag (mouse)
	F2ENDSTOP-Rev	5' GGGG AC CAC TTT GTA CAA GAA AGC TGG GTC <u>TCA</u> GAG GTT CTT GTC CAA GCAGGGT 3'	
pDONR-FARP2-del/Mut	F2STARTMET-For	5' GGGG ACA AGT TTG TAC AAA AAA GCA GGC TTC <u>ATG</u> GGA GAG ATA GAA GGA ACA TAC 3'	pCDNA3.1+FARP2-del/Mut nter flag (mouse)
	F2ENDSTOP-Rev	5' GGGG AC CAC TTT GTA CAA GAA AGC TGG GTC <u>TCA</u> GAG GTT CTT GTC CAA GCAGGGT 3'	
pDONR-Rock2-DN#1	R2-1STARTMET-For	5' GGGG ACA AGT TTG TAC AAA AAA GCA GGC TTC ACC <u>ATG</u> GAA AAA GAG AAG ATC ATG AAA GAG 3'	pCDNA3-ROCK2-FL (human) (Sebbagh <i>et al</i> , 2005)
	R2-1ENDSTOP-Rev	5' GGG GAC CAC TTT GTA CAA GAA AGC TGG GTC <u>TTA</u> GCT AGG TTT GTT TGG GGC AAG 3'	
Rock2-DN#1 mutagenesis (Asn-Lys to Thr-Thr)			
Construct name		Primer sequence	Template
pDONR-Rock2-DN#2		5' CTC AAA ACT CAA GCT GTG <u>ACT</u> <u>ACG</u> TTG GCT GAG ATC ATG AAT CG 3'	pDONR-Rock2-DN#1
Construct name	Primer name	Primer sequence	Template
pDONR-FARP1-FL	F1STARTMET-For	5' GGGG ACA AGT TTG TAC AAA AAA GCA GGC TTC <u>ATG</u> GGA GAA ATA GAG CAG AGG 3'	pCDNA3.1+FARP1-FL nter flag (human)
	F1ENDSTOP-Rev	5' GGG GAC CAC TTT GTA CAA GAA AGC TGG GTC <u>TCA</u> ATA CAC AAG AGA CTC TTT GTG 3'	
pDONR-FARP2-FL	F2STARTMET-For	5' GGGG ACA AGT TTG TAC AAA AAA GCA GGC TTC <u>ATG</u> GGA GAG ATA GAA GGA ACA TAC 3'	pCDNA3.1+FARP2-FL nter flag (mouse)
	F2ENDSTOP-Rev	5' GGGG AC CAC TTT GTA CAA GAA AGC TGG GTC <u>TCA</u> GAG GTT CTT GTC CAA GCAGGGT 3'	
pDONR-FARP2-Mut	F2STARTMET-For	5' GGGG ACA AGT TTG TAC AAA AAA GCA GGC TTC <u>ATG</u> GGA GAG ATA GAA GGA ACA TAC 3'	pCDNA3.1+FARP2-Mut nter flag (mouse)
	F2ENDSTOP-Rev	5' GGGG AC CAC TTT GTA CAA GAA AGC TGG GTC <u>TCA</u> GAG GTT CTT GTC CAA GCAGGGT 3'	
pDONR-FARP2-Del	F2STARTMET-For	5' GGGG ACA AGT TTG TAC AAA AAA GCA GGC TTC <u>ATG</u> GGA GAG ATA GAA GGA ACA TAC 3'	pCDNA3.1+FARP2-del nter flag (mouse)
	F2ENDSTOP-Rev	5' GGGG AC CAC TTT GTA CAA GAA AGC TGG GTC <u>TCA</u> GAG GTT CTT GTC CAA GCAGGGT 3'	
pDONR-FARP2-del/Mut	F2STARTMET-For	5' GGGG ACA AGT TTG TAC AAA AAA GCA GGC TTC <u>ATG</u> GGA GAG ATA GAA GGA ACA TAC 3'	pCDNA3.1+FARP2-del/Mut nter flag (mouse)
	F2ENDSTOP-Rev	5' GGGG AC CAC TTT GTA CAA GAA AGC TGG GTC <u>TCA</u> GAG GTT CTT GTC CAA GCAGGGT 3'	
pDONR-Rock2-DN#1	R2-1STARTMET-For	5' GGGG ACA AGT TTG TAC AAA AAA GCA GGC TTC ACC <u>ATG</u> GAA AAA GAG AAG ATC ATG AAA GAG 3'	pCDNA3-ROCK2-FL (human) (Sebbagh <i>et al</i> , 2005)
	R2-1ENDSTOP-Rev	5' GGG GAC CAC TTT GTA CAA GAA AGC TGG GTC <u>TTA</u> GCT AGG TTT GTT TGG GGC AAG 3'	

Lentiviral Infection of Caco-2 single cells and cysts

Caco-2 was infected at a MOI = 1. Lentiviral particles were added to Caco-2 cells in suspension (2×10^5 cells/ml) in complete medium supplemented with protamine (8 µg/ml) and were left to adhere and grow for 3 days. pGIPZ and pLKO-transduced Caco-2 cells were trypsinized and selected in puromycin (6 µg/ml)-supplemented complete medium. Cysts were transduced with 1.10^4 to 1.10^5 per ml of lentiviral particles to reach a mosaic or acute transduction of the cyst. Briefly, after 3 days of Caco-2 cyst morphogenesis in Ibidi chambers, the 2% Matrigel (BD, 354230) supernatant medium was removed and replaced with complete medium supplemented with Cholera Toxin (0.05 µg/ml) mixed with the appropriate amount of lentiviral particles. The Ibidi was kept 24 h at 37°C before fixation or performing the invasion assay.

Immunofluorescence (IF) and antibodies

Samples were washed twice in PBS supplemented with calcium (0.1 mM) and magnesium (1 mM) (PBS-CM) and fixed in PFA (4%) diluted in PBS-CM for 10 min for coverslips and tissue sections, 30 min for Caco-2 cysts and 45 min for organoids. Permeabilization was performed in PBS supplemented with 0.1% Triton X-100 during 10 min for coverslips and tissue sections, 0.5% Triton X-100 during 30 min for Caco-2 cysts and organoids. Samples were washed and incubated with primary antibodies diluted in PBS with 10% FBS (supplemented with 0.1% Triton X-100 for organoids) 1 h at room temperature for coverslips, overnight at 4°C for Caco-2 cysts, tissue section and organoids. Then, samples were washed in PBS-T (PBS–Tween-20 0.05% for Caco-2 cysts and organoids) and incubated with secondary antibodies diluted in antibody diluent at least 45 min at room temperature. After washing, the coverslips and tissue sections were mounted using Fluoromount-G (Southern Biotech, 0100-01).

The following primary antibodies were used at the indicated dilutions: ROCK1 (1:1,000, Abcam, ab134181), ROCK2 (1:1,000, Santa Cruz, sc-5561), E-cadherin (1:100, Abcam, ab1416), E-cadherin (1:100, Cell Signaling Technology, 3195S), phospho-ERM (1:100, Cell Signaling Technology, 3149), ezrin (1:100, BD Biosciences, 610603), ZO-1 (1:200, Invitrogen, 40-2300), beta-catenin (1:100, Thermofisher, MA1-300), vimentin (1:100, Thermofisher, PA1-16759), alpha-catenin (1:100, Sigma-Aldrich, C2081), Alexa Fluor™ Phalloidin 488 (1:200, Thermofisher, A12379).

Primary CRC sections staining and antibodies

Colorectal cancer specimens were immunostained with mouse monoclonal antibodies against E-cadherin (4A2C7, Invitrogen), vimentin (Thermofisher, PA1-16759), EpCam (1:100, Thermofisher, MA5-12436) and villin (1:100, Cell Signalling Technology, R814). For immunohistochemistry, stainings were performed with Ventana BenchMark XT immunostainer (Ventana Medical Systems, Tucson, AZ) utilizing UltraView DABv3 kit (Ventana, 7600-500). The chromogene was 3,3'-diaminobenzidine (DAB) in all the stainings. For immunofluorescence, stainings were performed as described for organoids.

Microscopy acquisition, live imaging and software-based quantification

Images were acquired using an Olympus Epifluorescence inverted X73 microscope, a confocal SpinningDisk CSU-W1 (Yokogawa) with a ZylasCMOC camera piloted with an Olympus X83 or a transmission electron microscope Libra 120 (Carl Zeiss).

Patients' specimens and Caco-2 cyst

Patients' specimens and Caco-2 cyst behaviours in 3D culture were imaged for up to 6 days by DIC time-lapse microscopy with motorized stage, temperature and CO2 controllers.

Quantitative IF images analysis

The invasion rate of the Caco-2 cysts invading into the adapted 3D Boyden chamber invasion assay was automatically quantified using the automated segmentation function of metamorph software.

Linescan analysis

Following Caco-2 cells transfection with pEGFP-FARP2, Metamorph software was used to trace lines crossing the cell–cell contact of fixed Caco-2 cells plated on 2D coverslips overexpressing GFP-FARP2 and stained for ZO-1 junctional protein. The quantification has been performed on 71 cells expressing GFP-FARP2-FL from 3 independent experiments. For each cell, between 10 and 15 regions (12 pixels wide) were drawn across the plasma membrane based on the endogenous ZO-1 staining using Metamorph. The fluorescence intensities were extracted for both channels (red (ZO-1) and the green (GFP-FARP2)). Importantly, the images were acquired at a constant exposure time for each staining (ZO-1 and GFP-FARP2). Average fluorescence intensity was calculated from at least 10 lines of 20 µm around each cell. The ratio of GFP-FARP2:ZO-1 maximum intensities was calculated.

Image display

Images were scaled relative to minimum and maximum pixel intensity of the image (non-linear adjustment (Gamma) was not used).

Rac-GTP Pull-down from tridimensional cultures

Caco-2 cysts were formed on 22-cm² culture dishes: briefly, 22-cm² dishes were coated with the Matrigel/Collagen-I (Corning, 354236) mix (110 µl/dish) prepared as described in the “Caco-2 cyst morphogenesis” section (described below) and Caco-2 cells (1.10^6 cell/ml) resuspended in complete medium supplemented with 2% Matrigel and cholera toxin (0.01 µg/ml) were added on top of the coating. After 3 days, Caco-2 cysts were treated with Y27632 (12 h, 25 µM) or with H1152 (16 h, 2 µM). Caco-2 cysts were then incubated 15 min with 2 mg/ml of collagenase (Sigma-Aldrich, C2139) in DMEM. The collagenase digestion was terminated by addition of complete medium and the cysts washed twice with ice-cold PBS supplemented with MgCl₂ (25 mM). Caco-2 cysts were scraped from dish in ice-cold PBS-MgCl₂, transferred to tubes and separated from the matrix by pelleting through 3 successive centrifugations of 1 min at 1,500 rpm. Retrieved Caco-2

cysts were then lysed in lysis buffer (50 mM Tris–HCl pH 7.5, 1% Triton X-100, 25 mM MgCl₂, 500 mM NaCl, 40 mM Na pyrophosphate, 1 mM NaVO₄, 2 mM phenylmethylsulphonyl fluoride (PMSF), 0.025% deoxycholate, 10 µg/ml aprotinin, 10 µg/ml leupeptin). Lysates were clarified by centrifugation, and equal amounts of protein lysates were incubated with 20 µl of purified glutathione S-transferase (GST)–CRIB immobilized on glutathione–Sephadex beads (17-0756-01, GE Healthcare) for 1 h rocking at 4°C. The beads were washed and incubated with SDS sample buffer (62.5 mM Tris–HCl pH 6.8, 10% glycerol, 0.002% bromophenol blue, 2% SDS and 5% β-mercaptoethanol) and boiled for 10 min. The samples were analysed for Rac1 pull-down by Western blot using an anti-Rac1 antibody (1:500; Cell Signaling, Beverly, MA).

Co-Immunoprecipitation

Caco-2 cells were transfected with plasmids expressing GFP–ROCK2DN#1 or GFP–ROCK2DN#2, lysed after 48 h with lysis buffer. Protein lysates were clarified by centrifugation, and equal amounts of protein lysates were incubated with GFP-trap® beads (gta-10; ChromoTek). The beads were then washed with lysis buffer and incubated 10 min at 95°C in SDS sample buffer before Western blot analysis with anti-ROCK1, anti-ROCK2 and anti-eGFP antibodies.

Western Blot and antibodies

Appropriately treated cells were lysed in lysis buffer and equal amount of proteins were boiled for 10 min in SDS sample buffer. The samples were subjected to SDS–polyacrylamide gel electrophoresis (PAGE) using precast acrylamide gels (ThermoFisher, NP0335BOX), and proteins were transferred to nitrocellulose membranes. Membranes were incubated for 30 min in Blocking solution (Tris-buffered saline (TBS) containing 0.1% Tween-20, 3% BSA or 5% milk) and further incubated with the appropriate primary antibody diluted in Blocking solution at 4°C overnight. The membranes were then washed three times with TBS–Tween (0.1%) and incubated for 45 min with secondary antibody conjugated to horseradish peroxidase (HRP). Bound antibodies were detected with enhanced chemiluminescence.

The following primary antibodies were used at the indicated dilutions: HSC70 (1:4000, Santa Cruz, sc-7298), GAPDH–HRP (1:10,000, Abcam, ab9482), ROCK1 (1:1,000, Abcam, ab134181), ROCK2 (1:1,000, Santa Cruz, sc-5561), FARP1 (1:100, Santa Cruz, sc-293249), FARP2 (1:50, Santa Cruz sc-390744), GFP (1:1,000 Santa Cruz, sc-8334), eGFP (1:1,000, Covance), RAC1 (1:500, BD Bioscience, 610650).

ROCK2 expression data

ROCK2 mRNA expression was evaluated in the large Affymetrix U133Plus gene expression data set GSE33582 from (Marisa et al 2013) which includes profiles from 566 colon tumours and 19 non-tumour tissues (NT). The values of the two probesets corresponding to ROCK2 gene were average, and the value was discretized relatively to the expression of ROCK2 in non-tumour tissues (tumours with values inferior to the 1st decile (7.6) of the expression in NT

were defined as tumours with a down-regulation of ROCK2). Overall survival curves were obtained using Kaplan–Meier estimates and differences between survival distributions were assessed by a log-rank test with an end point at 3 and 5 years.

Statistical analyses

The normal distribution of the protrusive phenotype in patient explants and cell lines in control condition was verified using the Shapiro–Wilk normality test. Parametric, paired and unpaired two-tailed *t*-tests were performed to determine whether the difference between control and treated groups was significantly different in their mean value using Prism 6. All errors indicated in the text are SEM.

Expanded View for this article is available online.

Acknowledgements

This work is dedicated to the memory of Alan Hall, an inspiring scientist and mentor. We thank Pr. Xuewu Zhang (University of Texas, USA) for providing us with the FARP1 and FARP2 constructs (He et al, 2013) which we used to generate lentiviral-based expression vectors, Pr. Yoshimi Takai (Kobe University, Japan) for the pEGFP–FARP2, Fatiha Sangar–Mavouna for cloning the human version of the ROCK2 constructs published by Amano et al and Ms U. Schultz for technical assistance with tumour samples processing. We thank the members of the Jaulin lab and Digestive Cancer Unit for discussion. We thank T. Omelchenko and S. Deborde for critical reading of the manuscript. This work was supported by the CNRS/INSERM ATIP-AVENIR programme, the Gustave Roussy foundation (Natixis), the INCA PLBIO and the LNCC comité IDF support to FJ, the French government MESR PhD fellowship and “Fondation pour la recherche medicale” (FDT20160435539) fourth-year PhD fellowship to FL, “Roulons pour le colon” and “Parrainez un chercheur” fund raising to OZ and RL.

Author contributions

FL designed, performed, analysed experiments and wrote the manuscript. The following experiments were performed by JR (pull-downs), RL (CRC explants) ZAT (siRNAs Myosin-II), OZ (organoids) FJ and JV (siRNA screens). PD, J-YS, FP, JA, DG and MG provided clinical samples and performed histological analyses. LM performed gene expression analyses from specimens provided by VB and DM. AH supported the siRNA screens. FJ conceived the project, designed the research, supervised the experimental design and wrote the manuscript. All provided intellectual input.

Conflict of interest

The authors declare that they have no conflict of interest.

References

- Aiello NM, Brabletz T, Kang Y, Nieto MA, Weinberg RA, Stanger BZ (2017) Upholding a role for EMT in pancreatic cancer metastasis. *Nature* 547: E7–E8
- Alexander S, Koehl GE, Hirschberg M, Geissler EK, Friedl P (2008) Dynamic imaging of cancer growth and invasion: a modified skin-fold chamber model. *Histochem Cell Biol* 130: 1147–1154
- Amano A, Piotrowski T (2008) Wnt/β-catenin and Fgf signaling control collective cell migration by restricting chemokine receptor expression. *Dev Cell* 15: 749–761

- Amano M, Chihara K, Nakamura N, Kaneko T, Matsuura Y, Kaibuchi K (1999) The COOH terminus of Rho-kinase negatively regulates Rho-kinase activity. *J Biol Chem* 274: 32418–32424
- Amano M, Hamaguchi T, Shohag MH, Kozawa K, Kato K, Zhang X, Yura Y, Matsuura Y, Kataoka C, Nishioka T et al (2015) Kinase-interacting substrate screening is a novel method to identify kinase substrates. *J Cell Biol* 209: 895–912
- Bianco A, Poukkula M, Cliffe A, Mathieu J, Luque CM, Fulga TA, Rørth P (2007) Two distinct modes of guidance signalling during collective migration of border cells. *Nature* 448: 362–365
- Bronsart P, Enderle-Ammour K, Bader M, Timme S, Kuehs M, Csanadi A, Kayser G, Kohler I, Bausch D, Hoeppner J et al (2014) Cancer cell invasion and EMT marker expression: a three-dimensional study of the human cancer-host interface. *J Pathol* 234: 410–422
- Cai D, Chen S-C, Prasad M, He L, Wang X, Choismel-Cadamuro V, Sawyer JK, Danuser G, Montell DJ (2014) Mechanical feedback through E-cadherin promotes direction sensing during collective cell migration. *Cell* 157: 1146–1159
- Calon A, Lonardo E, Berenguer-Llargo A, Espinet E, Hernando-Momblona X, Iglesias M, Sevillano M, Palomo-Ponce S, Tauriello DVF, Byrom D et al (2015) Stromal gene expression defines poor-prognosis subtypes in colorectal cancer. *Nat Genet* 47: 320–329
- Chaffer CL, Juan BPS, Lim E, Weinberg RA (2016) EMT, cell plasticity and metastasis. *Cancer Metastasis Rev* 35: 645–654
- Cheadle L, Biederer T (2012) The novel synaptogenic protein Farp1 links postsynaptic cytoskeletal dynamics and transsynaptic organization. *J Cell Biol* 199: 985–1001
- Cheung KJ, Gabrielson E, Werb Z, Ewald AJ (2013) Collective invasion in breast cancer requires a conserved basal epithelial program. *Cell* 155: 1639–1651
- Cheadle L, Biederer T (2014) Activity-dependent regulation of dendritic complexity by semaphorin 3A through Farp1. *J Neurosci Off J Soc Neurosci* 34: 7999–8009
- Cheung KJ, Ewald AJ (2016) A collective route to metastasis: seeding by tumor cell clusters. *Science* 352: 167–169
- Croft DR, Sahai E, Mavria G, Li S, Tsai J, Lee WMF, Marshall CJ, Olson MF (2004) Conditional ROCK activation *in vivo* induces tumor cell dissemination and angiogenesis. *Cancer Res* 64: 8994–9001
- Duchek P, Somogyi K, Jékely G, Beccari S, Rørth P (2001) Guidance of cell migration by the *Drosophila* PDGF/VEGF receptor. *Cell* 107: 17–26
- Dupont S, Morsut L, Aragona M, Enzo E, Giulitti S, Cordenonsi M, Zanconato F, Le Dıgabel J, Forcato M, Bicciato S et al (2011) Role of YAP/TAZ in mechanotransduction. *Nature* 474: 179–183
- Durdu S, Iskar M, Revenu C, Schieber N, Kunze A, Bork P, Schwab Y, Gilmour D (2014) Luminal signalling links cell communication to tissue architecture during organogenesis. *Nature* 515: 120–124
- Durgan J, Kaji N, Jin D, Hall A (2011) Par6B and atypical PKC regulate mitotic spindle orientation during epithelial morphogenesis. *J Biol Chem* 286: 12461–12474
- Ellenbroek SJJ, Iden S, Collard JG (2012) The Rac activator Tiam1 is required for polarized protrusional outgrowth of primary astrocytes by affecting the organization of the microtubule network. *Small GTPases* 3: 4–14
- Enderle-Ammour K, Bader M, Ahrens TD, Franke K, Timme S, Csanadi A, Hoeppner J, Kulemann B, Maurer J, Reiss P et al (2017) Form follows function: morphological and immunohistological insights into epithelial-mesenchymal transition characteristics of tumor buds. *Tumour Biol J Int Soc Oncodevelopmental Biol Med* 39: 1010428317705501
- Even-Ram S, Doyle AD, Conti MA, Matsumoto K, Adelstein RS, Yamada KM (2007) Myosin IIA regulates cell motility and actomyosin-microtubule crosstalk. *Nat Cell Biol* 9: 299–309
- Ewald AJ, Huebner RJ, Palsdottir H, Lee JK, Perez MJ, Jorgens DM, Tauscher AN, Cheung KJ, Werb Z, Auer M (2012) Mammary collective cell migration involves transient loss of epithelial features and individual cell migration within the epithelium. *J Cell Sci* 125: 2638–2654
- Ferlay J, Soerjomataram I, Dikshit R, Eser S, Mathers C, Rebelo M, Parkin DM, Forman D, Bray F (2015) Cancer incidence and mortality worldwide: sources, methods and major patterns in GLOBOCAN 2012. *Int J Cancer* 136: E359–E386
- Fischer RS, Gardel M, Ma X, Adelstein RS, Waterman CM (2009) Local cortical tension by myosin II guides 3D endothelial cell branching. *Curr Biol* 19: 260–265
- Fischer KR, Durrans A, Lee S, Sheng J, Li F, Wong STC, Choi H, El Rayes T, Ryu S, Troeger J et al (2015) Epithelial-to-mesenchymal transition is not required for lung metastasis but contributes to chemoresistance. *Nature* 527: 472–476
- Fleming M, Ravula S, Tatishchev SF, Wang HL (2012) Colorectal carcinoma: pathologic aspects. *J Gastrointest Oncol* 3: 153–173
- Friedl P, Noble PB, Walton PA, Laird DW, Chauvin PJ, Tabah RJ, Black M, Zanker KS (1995) Migration of coordinated cell clusters in mesenchymal and epithelial cancer explants *in vitro*. *Cancer Res* 55: 4557–4560
- Friedl P (2004) Prespecification and plasticity: shifting mechanisms of cell migration. *Curr Opin Cell Biol* 16: 14–23
- Friedl P, Alexander S (2011) Cancer invasion and the microenvironment: plasticity and reciprocity. *Cell* 147: 992–1009
- Friedl P, Locker J, Sahai E, Segall JE (2012) Classifying collective cancer cell invasion. *Nat Cell Biol* 14: 777–783
- Giampieri S, Manning C, Hooper S, Jones L, Hill CS, Sahai E (2009) Localized and reversible TGF β signalling switches breast cancer cells from cohesive to single cell motility. *Nat Cell Biol* 11: 1287–1296
- Guinney J, Dienstmann R, Wang X, de Reyniès A, Schlicker A, Soneson C, Marisa L, Roepman P, Nyamundanda G, Angelino P et al (2015) The consensus molecular subtypes of colorectal cancer. *Nat Med* 21: 1350–1356
- Haas P, Gilmour D (2006) Chemokine signaling mediates self-organizing tissue migration in the zebrafish lateral line. *Dev Cell* 10: 673–680
- He X, Kuo Y-C, Rosche TJ, Zhang X (2013) Structural basis for autoinhibition of the guanine nucleotide exchange factor FARP2. *Structure* 21: 355–364
- Hidalgo-Carcedo C, Hooper S, Chaudhry SI, Williamson P, Harrington K, Leitinger B, Sahai E (2011) Collective cell migration requires suppression of actomyosin at cell-cell contacts mediated by DDR1 and the cell polarity regulators Par3 and Par6. *Nat Cell Biol* 13: 49–58
- Hoogwater FJH, Nijkamp MW, Smakman N, Steller EJA, Emmink BL, Westendorp BF, Raats DAE, Sprick MR, Schaefer U, Van Houdt WJ et al (2010) Oncogenic K-Ras turns death receptors into metastasis-promoting receptors in human and mouse colorectal cancer cells. *Gastroenterology* 138: 2357–2367
- Itoh K, Yoshioka K, Akedo H, Uehata M, Ishizaki T, Narumiya S (1999) An essential part for Rho-associated kinase in the transcellular invasion of tumor cells. *Nat Med* 5: 221–225
- Julien S, Merino-Trigo A, Lacroix L, Pocard M, Goéré D, Mariani P, Landron S, Bigot L, Nemati F, Dartigues P et al (2012) Characterization of a large panel of patient-derived tumor xenografts representing the clinical heterogeneity of human colorectal cancer. *Clin Cancer Res* 18: 5314–5328
- Khalil AA, Ilina O, Gritsenko PG, Bult P, Span PN, Friedl P (2017) Collective invasion in ductal and lobular breast cancer associates with distant metastasis. *Clin Exp Metastasis* 1–9

- Kim H, Verhaak RGW (2015) Transcriptional mimicry by tumor-associated stroma. *Nat Genet* 47: 3255
- Konen J, Summerbell E, Dwivedi B, Galior K, Hou Y, Rusnak L, Chen A, Saltz J, Zhou W, Boise LH et al (2017) Image-guided genomics of phenotypically heterogeneous populations reveals vascular signalling during symbiotic collective cancer invasion. *Nat Commun* 8: 15078
- Koyano Y, Kawamoto T, Shen M, Yan W, Noshiro M, Fujii K, Kato Y (1997) Molecular cloning and characterization of CDEP, a novel human protein containing the ezrin-like domain of the band 4.1 superfamily and the Dbl homology domain of Rho guanine nucleotide exchange factors. *Biochem Biophys Res Commun* 241: 369–375
- Koyano Y, Kawamoto T, Kikuchi A, Shen M, Kuruta Y, Tsutsumi S, Fujimoto K, Noshiro M, Fujii K, Kato Y (2001) Chondrocyte-derived ezrin-like domain containing protein (CDEP), a rho guanine nucleotide exchange factor, is inducible in chondrocytes by parathyroid hormone and cyclic AMP and has transforming activity in NIH3T3 Cells. *Osteoarthritis Cartilage* 9(Suppl 1): S64–S68
- Krebs AM, Mitschke J, Lasier Losada M, Schmalhofer O, Boerries M, Busch H, Boettcher M, Mougiakakos D, Reichardt W, Bronsert P et al (2017) The EMT-activator Zeb1 is a key factor for cell plasticity and promotes metastasis in pancreatic cancer. *Nat Cell Biol* 19: 518–529
- Kubo T, Yamashita T, Yamaguchi A, Sumimoto H, Hosokawa K, Tohyama M (2002) A novel FERM domain including guanine nucleotide exchange factor is involved in Rac signaling and regulates neurite remodeling. *J Neurosci Off J Soc Neurosci* 22: 8504–8513
- Kwon S-H, Liu KD, Mostov KE (2014) Intercellular transfer of GPRC5B via exosomes drives HGF-mediated outward growth. *Curr Biol* 24: 199–204
- Lomakin AJ, Lee K-C, Han SJ, Bui DA, Davidson M, Mogilner A, Danuser G (2015) Competition for actin between two distinct F-actin networks defines a bistable switch for cell polarization. *Nat Cell Biol* 17: 1435–1445
- Marisa L, de Reyniès A, Duval A, Selves J, Gaub MP, Vescovo L, Etienne-Grimaldi MC, Schiappa R, Guenot D, Ayadi M et al (2015) Gene expression classification of colon cancer into molecular subtypes: characterization, validation, and prognostic value. *PLoS Med* 10: e1001453
- Matano M, Date S, Shimokawa M, Takano A, Fujii M, Ohta Y, Watanabe T, Kanai T, Sato T (2015) Modeling colorectal cancer using CRISPR-Cas9-mediated engineering of human intestinal organoids. *Nat Med* 21: 256–262
- McCorry AMB, Loughrey MB, Longley DB, Lawler M, Dunne PD (2018) Epithelial-to-mesenchymal transition signature assessment in colorectal cancer quantifies tumour stromal content rather than true transition. *J Pathol* 246: 422–426
- Migeotte I, Omelchenko T, Hall A, Anderson KV (2010) Rac1-dependent collective cell migration is required for specification of the anterior-posterior body axis of the mouse. *PLoS Biol* 8: e1000442
- Miyamoto Y, Yamauchi J, Itoh H (2003) Src kinase regulates the activation of a novel FGD-1-related Cdc42 guanine nucleotide exchange factor in the signaling pathway from the endothelin A receptor to JNK. *J Biol Chem* 278: 29890–29900
- Mlechkovich G, Peng S-S, Shacham V, Martinez E, Gokhman I, Minis A, Tran TS, Yaron A (2014) Distinct cytoplasmic domains in plexin-A4 mediate diverse responses to semaphorin 3A in developing mammalian neurons. *Sci Signal* 7: ra24
- Narumiya S, Tanji M, Ishizaki T (2009) Rho signaling, ROCK and mDia1, in transformation, metastasis and invasion. *Cancer Metastasis Rev* 28: 65–76
- Nieto MA, Huang RY-J, Jackson RA, Thiery JP (2016) EMT: 2016. *Cell* 166: 21–45
- Ohta Y, Hartwig JH, Stossel TP (2006) FilGAP, a Rho- and ROCK-regulated GAP for Rac binds filamin A to control actin remodelling. *Nat Cell Biol* 8: 803–814
- Omelchenko T, Vasiliev JM, Gelfand IM, Feder HH, Bonder EM (2003) Rho-dependent formation of epithelial “leader” cells during wound healing. *Proc Natl Acad Sci USA* 100: 10788–10793
- Omelchenko T, Hall A (2012) Myosin-IXA regulates collective epithelial cell migration by targeting RhoGAP activity to cell-cell junctions. *Curr Biol* 22: 278–288
- Omelchenko T, Rabadan MA, Hernández-Martínez R, Grego-Bessa J, Anderson KV, Hall A (2014) β -Pix directs collective migration of anterior visceral endoderm cells in the early mouse embryo. *Genes Dev* 28: 2764–2777
- Osmani N, Vitale N, Borg J-P, Etienne-Manneville S (2006) Scrib controls Cdc42 localization and activity to promote cell polarization during astrocyte migration. *Curr Biol* 16: 2395–2405
- Osmani N, Peglion F, Chavrier P, Etienne-Manneville S (2010) Cdc42 localization and cell polarity depend on membrane traffic. *J Cell Biol* 191: 1261–1269
- Pino MS, Chung DC (2010) The chromosomal instability pathway in colon cancer. *Gastroenterology* 138: 2059–2072
- Prall F, Nizze H, Barten M (2005) Tumour budding as prognostic factor in stage I/II colorectal carcinoma. *Histopathology* 47: 17–24
- Prall F, Ostwald C, Linnebacher M (2009) Tubular invasion and the morphogenesis of tumor budding in colorectal carcinoma. *Hum Pathol* 40: 1510–1512
- Puisieux A, Brabletz T, Caramel J (2014) Oncogenic roles of EMT-inducing transcription factors. *Nat Cell Biol* 16: 488–494
- Rath N, Munro J, Cutiongco MF, Jagieho A, Gadegaard N, McGarry L, Unbekandt M, Michalopoulou E, Kamphorst JJ, Sumpton D et al (2018) Rho kinase inhibition by AT13148 blocks pancreatic ductal adenocarcinoma invasion and tumor growth. *Cancer Res* 78: 3321–3336
- Reffay M, Parrini MC, Cochet-Escartin O, Ladoux B, Buguin A, Coscoy S, Amblard F, Camonis J, Silberzan P (2014) Interplay of RhoA and mechanical forces in collective cell migration driven by leader cells. *Nat Cell Biol* 16: 217–223
- Revenu C, Streichen S, Donà E, Lecaudey V, Hufnagel L, Gilmour D (2014) Quantitative cell polarity imaging defines leader-to-follower transitions during collective migration and the key role of microtubule-dependent adherens junction formation. *Development* 141: 1282–1291
- Ridley AJ (2015) Rho GTPase signalling in cell migration. *Curr Opin Cell Biol* 36: 103–112
- Sadok A, Marshall CJ (2014) Rho GTPases: masters of cell migration. *Small GTPases* 5: e29710
- Sadok A, McCarthy A, Caldwell J, Collins I, Garrett MD, Yeo M, Hooper S, Sahai E, Kuemper S, Mardakheh FK et al (2015) Rho kinase inhibitors block melanoma cell migration and inhibit metastasis. *Cancer Res* 75: 2272–2284
- Sahai E, Olson MF, Marshall CJ (2001) Cross-talk between Ras and Rho signalling pathways in transformation favours proliferation and increased motility. *EMBO J* 20: 755–766
- Sahai E, Marshall CJ (2003) Differing modes of tumour cell invasion have distinct requirements for Rho/ROCK signalling and extracellular proteolysis. *Nat Cell Biol* 5: 711–719
- Samuel MS, Lopez JL, McGhee EJ, Croft DR, Strachan D, Timpson P, Munro J, Schröder E, Zhou J, Brunton VG et al (2011) Actomyosin-mediated cellular tension drives increased tissue stiffness and β -catenin activation to induce epidermal hyperplasia and tumor growth. *Cancer Cell* 19: 776–791
- Sanz-Moreno V, Gadea G, Ahn J, Paterson H, Marra P, Pinner S, Sahai E, Marshall CJ (2008) Rac activation and inactivation control plasticity of tumor cell movement. *Cell* 135: 510–523
- Sanz-Moreno V, Gaggioli C, Yeo M, Albrengues J, Wallberg F, Virois A, Hooper S, Mitter R, Féral CC, Cook M et al (2011) ROCK and JAK1 signaling

- cooperate to control actomyosin contractility in tumor cells and stroma. *Cancer Cell* 20: 229–245
- Sato T, Clevers H (2013) Growing self-organizing mini-guts from a single intestinal stem cell: mechanism and applications. *Science* 340: 1190–1194
- Schramek D, Sendoel A, Segal JP, Beronja S, Heller E, Oristian D, Reva B, Fuchs E (2014) Direct *in vivo* RNAi screen unveils myosin IIa as a tumor suppressor of squamous cell carcinomas. *Science* 343: 309–313
- Sebbagh M, Hamelin J, Bertoglio J, Solary E, Bréard J (2005) Direct cleavage of ROCK II by granzyme B induces target cell membrane blebbing in a caspase-independent manner. *J Exp Med* 201: 465–471
- Spaderna S, Schmalhofer O, Wahlbuhl M, Dimmler A, Bauer K, Sultan A, Hlubek F, Jung A, Strand D, Eger A et al (2008) The transcriptional repressor ZEB1 promotes metastasis and loss of cell polarity in cancer. *Cancer Res* 68: 537–544
- Takegahara N, Kang S, Nojima S, Takamatsu H, Okuno T, Kikutani H, Toyofuku T, Kumanogoh A (2010) Integral roles of a guanine nucleotide exchange factor, FARP2, in osteoclast podosome rearrangements. *FASEB J* 24: 4782–4792
- Thiery JP, Acloque H, Huang RY, Nieto MA (2009) Epithelial-mesenchymal transitions in development and disease. *Cell* 139: 871–890
- Toyofuku T, Yoshida J, Sugimoto T, Zhang H, Kumanogoh A, Hori M, Kikutani H (2005) FARP2 triggers signals for Semaphorin3A-mediated axonal repulsion. *Nat Neurosci* 8: 1712–1719
- Tsuji T, Ishizaki T, Okamoto M, Higashida C, Kimura K, Furuyashiki T, Arakawa Y, Birge RB, Nakamoto T, Hirai H et al (2002) ROCK and mDia1 antagonize in Rho-dependent Rac activation in Swiss 3T3 fibroblasts. *J Cell Biol* 157: 819–830
- Valastyan S, Weinberg RA (2011) Tumor metastasis: molecular insights and evolving paradigms. *Cell* 147: 275–292
- Vennin C, Rath N, Pajic M, Olson MF, Timpson P (2017) Targeting ROCK activity to disrupt and prime pancreatic cancer for chemotherapy. *Small GTPases* 3: 1–8
- Vicente-Manzanares M, Ma X, Adelstein RS, Horwitz AR (2009) Non-muscle myosin II takes centre stage in cell adhesion and migration. *Nat Rev Mol Cell Biol* 10: 778–790
- Vignjevic D, Schoumacher M, Gavert N, Janssen K-P, Jih G, Laé M, Louvard D, Ben-Ze'ev A, Robine S (2007) Fascin, a novel target of beta-catenin-TCF signaling, is expressed at the invasive front of human colon cancer. *Cancer Res* 67: 6844–6853
- Voorneveld PW, Kodach LL, Jacobs RJ, Liv N, Zonneville AC, Hoogenboom JP, Biemond I, Verspaget HW, Hommes DW, de Rooij K et al (2014) Loss of SMAD4 alters BMP signaling to promote colorectal cancer cell metastasis via activation of Rho and ROCK. *Gastroenterology* 147: 196–208.e13
- Wang X, He L, Wu YI, Hahn KM, Montell DJ (2010) Light-mediated activation reveals a key role for Rac in collective guidance of cell movement *in vivo*. *Nat Cell Biol* 12: 591–597
- Wellner U, Schubert J, Burk UC, Schmalhofer O, Zhu F, Sonntag A, Waldvogel B, Vannier C, Darling D, zur Hausen A et al (2009) The EMT-activator ZEB1 promotes tumorigenicity by repressing stemness-inhibiting microRNAs. *Nat Cell Biol* 11: 1487–1495
- Westcott JM, Pechtl AM, Maine EA, Dang TT, Esparza MA, Sun H, Zhou Y, Xie Y, Pearson GW (2015) An epigenetically distinct breast cancer cell subpopulation promotes collective invasion. *J Clin Invest* 125: 1927–1943
- Wolf K, Mazo I, Leung H, Engelke K, von Andrian UH, Deryugina EI, Strongin AY, Bröcker E-B, Friedl P (2003) Compensation mechanism in tumor cell migration. *J Cell Biol* 160: 267–277
- Yamaguchi N, Mizutani T, Kawabata K, Haga H (2015) Leader cells regulate collective cell migration via Rac activation in the downstream signaling of integrin β 1 and PI3K. *Sci Rep* 5: srep07656
- Yamane L, Scapulatempo-Neto C, Reis RM, Guimarães DP (2014) Serrated pathway in colorectal carcinogenesis. *World J Gastroenterol* 20: 2634–2640
- Ye X, Brabletz T, Kang Y, Longmore GD, Nieto MA, Stanger BZ, Yang J, Weinberg RA (2017) Upholding a role for EMT in breast cancer metastasis. *Nature* 547: E1–E3
- Zajac O, Raingeaud J, Libanje F, Lefebvre C, Sabino D, Martins I, Roy P, Benatar C, Canet-Jourdan C, Azorin P et al (2018) Tumour spheres with inverted polarity drive the formation of peritoneal metastases in patients with hypermethylated colorectal carcinomas. *Nat Cell Biol* 20: 296–306
- Zaritsky A, Tseng Y-Y, Rabadán MA, Krishna S, Overholtzer M, Danuser G, Hall A (2017) Diverse roles of guanine nucleotide exchange factors in regulating collective cell migration. *J Cell Biol* 216: 1543–1556
- Zheng X, Carstens JL, Kim J, Scheible M, Kaye J, Sugimoto H, Wu C-C, LeBleu VS, Kalluri R (2015a) EMT program is dispensable for metastasis but induces chemoresistance in pancreatic cancer. *Nature* 527: 525
- Zheng X, Carstens JL, Kim J, Scheible M, Kaye J, Sugimoto H, Wu C-C, LeBleu VS, Kalluri R (2015b) Epithelial-to-mesenchymal transition is dispensable for metastasis but induces chemoresistance in pancreatic cancer. *Nature* 527: 525–530
- Zhuang B, Su YS, Sockanathan S (2009) FARP1 promotes the dendritic growth of spinal motor neuron subtypes through transmembrane Semaphorin6A and PlexinA4 signaling. *Neuron* 61: 359–372